Computational and Experimental Design of Fe-Based Superalloys for Elevated-Temperature Applications

Peter K. Liaw[1], Zhenke Teng[1], Shenyan Huang[1], Chain T. Liu[2], Morris E. Fine[3], Gautam Ghosh[3], Mark D. Asta[4], and Gongyao Wang[1]

1. Department of Materials Science and Engineering, The University of Tennessee, Knoxville, TN 37996, USA
2. Department of Materials Engineering, Auburn University, Auburn, AL 36849, USA, and Department of Mechanical Engineering, Hong Kong Polytechnic University, Hung Hom, Kowloon, Hong Kong.
3. Department of Materials Science and Engineering, Northwestern University, Evanston, IL 60208-3108, USA
4. Department of Materials Science and Engineering, University of California, Berkeley, CA 94720, USA

06-03-2010

Acknowledgement

- This work is supported by The Department of Energy (DOE) Office of Fossil Energy Program, under Grant No. DE-FG26-09NT0008089, with Mr. Vito Cedro and Dr. Patricia Rawls as the program directors.

- The use of the Division of Scientific User Facilities is sponsored by the Office of Basic Energy Sciences, U.S. Department of Energy, Oak Ridge National Laboratory (ORNL).

- The use of the Advanced Photon Source at Argonne National Laboratory is supported by the U.S. Department of Energy, Office of Science, Office of Basic Energy Sciences, under Contract No. DE-AC02-06CH11357.

- The Los Alamos Neutron Science Center (LANSCE) is a national user facility funded by the U.S. Department of Energy, the Office of Basic Energy Science – Materials Science, under Contract No. W-7405-ENG-36 with the University of California.

- Dr. Carl McHargue, Director of Center for Materials Processing, University of Tennessee, provides matching funds.

Outline

- Introduction
- Critical Issues and Objectives
- System-Based Materials Design
- Computational and Experimental Results
  - First-Principles Calculations on Impurity Diffusivities in Ferritic Iron
  - Alloy Design and Fabrication
  - Ultra-Small-Angle X-ray Diffraction (USAXS) Characterization of NiAl-Type Precipitates
  - Atom-Probe-Tomography (APT) Characterization of Nanoscale NiAl-Type Precipitates
  - Creep Behavior
  - Ductility Study
- Conclusion
- Publications, Presentations, and Awards
- Future Work

Introduction (1)

- Why ferritic steels? Why not Ni-based alloys?
- 80% of all electricity generation in the world is by use of steam turbines. Low cost materials are required.

- The materials with good thermal conductivity and low thermal expansion are preferable for thick section components of the steam turbine.

	Thermal Expansion Coefficient [2]	**Thermal Conductivity** [3]	**Cost ($/ton)** [4]
Ferritic Steel	**1.0×10^{-5} K^{-1}**	**50 W/(m·K)**	**< $900**
Ni-based Superalloy	**1.8×10^{-5} K^{-1}**	**21 W/(m·K)**	**> $40K**

A rotor of a modern steam turbine, used in a power plant [1]

[1] http://en.wikipedia.org/wiki/Steam_turbine
[2] http://www.handyharmancanada.com/TheBrazingBook/comparis.htm
[3] http://en.wikipedia.org/wiki/List_of_thermal_conductivities
[4] http://www.ttiinc.com/page/ME_Materials

Introduction (2)

Why (Fe,Ni)Al-strengthened ferritic steels?

Phase	Structure	Lattice Parameter (nm)
α-Fe	Body-Centered-Cubic (BCC)	0.28665
NiAl	B2 (ordered BCC)	0.28864
FeAl	B2 (ordered BCC)	0.289

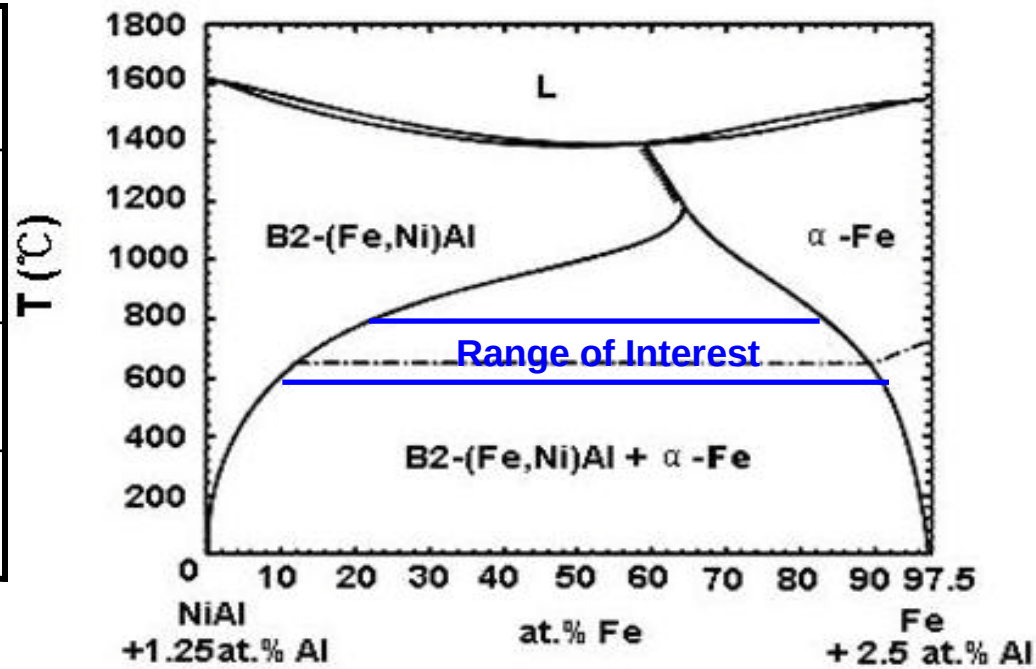

Ordered B2 (Fe, Ni)Al-type precipitates can form in a coherent-coplanar orientation, providing the possibility of achieving a Fe-based analogue to the Ni-based superalloys.

Critical Issues

- **Limited creep resistance at temperatures higher than 600 ºC**
- **Room-temperature ductility less than 1%**

$$\varepsilon_f = 6Dt / L^2$$

ε_f : the strain on the outer surface

D : the maximum deflection at the center of the strip (mm)

t : the thickness (mm)

L : the support span (mm)

Fe-10Al-10Cr-10Ni-3.4Mo-0.25Zr-0.005B (wt.%)

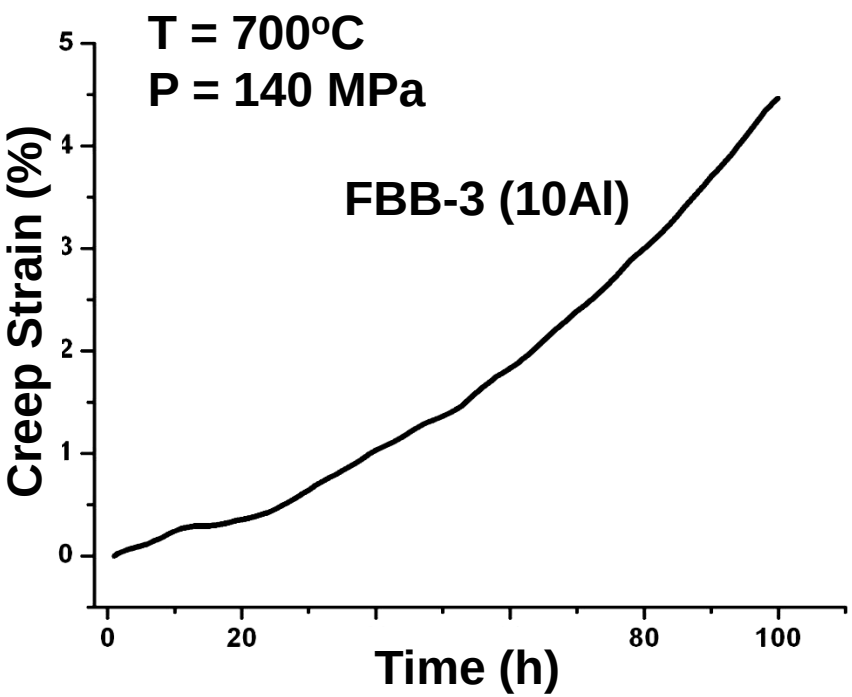

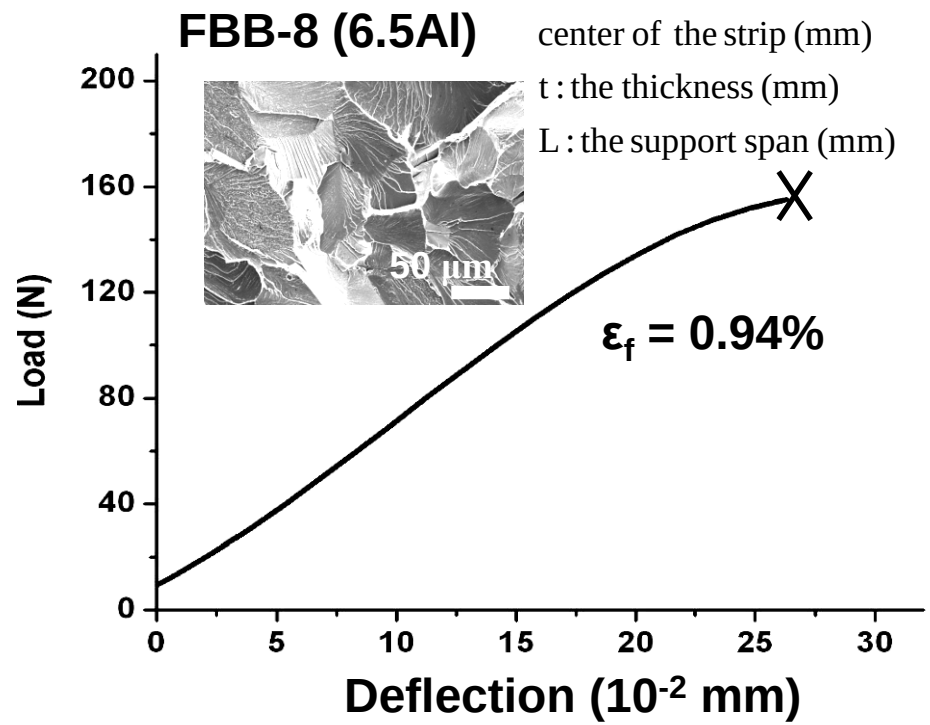

The creep strain reaches 5% after only 100 h

The room-temperature ductility is less than 1%, and the fracture mode is cleavage.

Objectives

- **Prediction of slow diffusing species in the Fe matrix by first-principles calculations.**

- **A steady-state creep rate of approximately 3 x 10^{-11} s^{-1} at a temperature of 760 ^{o}C and a stress level of 35 MPa.**

- **A tensile ductility of ~ 10% at room temperature for sufficient workability in as-cast and subsequent fabrication stages.**

- **Fundamental understanding of the effects of**

  (1) NiAl-precipitate microstructures (size, inter-particle spacing, and volume fraction) and
  (2) the compositions of both the precipitates and the matrix

  on the creep resistance and ductility of the NiAl-strengthened ferritic steel.

Systems-Based Materials Design

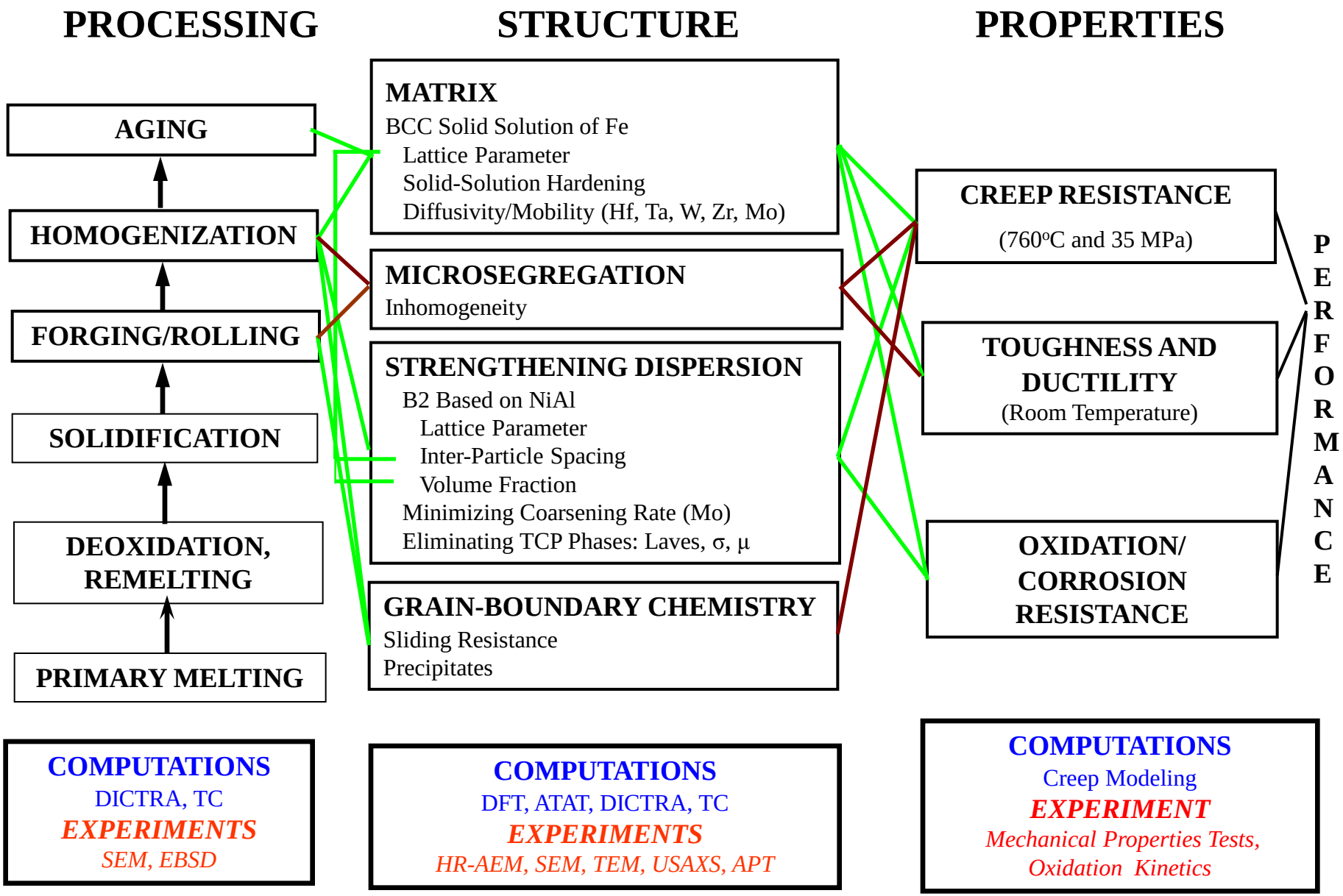

Computational Tools Used and to be Used in the Present Research

- **Electronic Density-Functional Theory (DFT)** code: Vienna Ab Initio Simulation Package (VASP):

  To calculate the total energy and electronic structure of many-body systems.
- **Alloy Theoretic Automated Toolkit (ATAT)**:

  To compute free energies for partially-ordered compounds and solid solutions.
- **Thermo-Calc (TC)**:

  To predict phase stability and phase equilibria as a function of composition and temperature in multi-component alloys.
- **DIffusion Controlled TRAnsformations (DICTRA)**:

  To simulate diffusion-controlled transformations in multi-component systems that involve multiple phases with simple geometries.

Experimental Tools Used and to be Used in the Present Research

- High-Resolution Analytical-Electron Microscopy (HR-AEM)
- Scanning-Electron Microscopy (SEM)
- Transmission-Electron Microscopy (TEM)
- Ultra-Small-Angle Synchrotron X-Ray Scattering (USAXS)
- Atom-Probe Tomography (APT)
- Differential-Scanning Calorimetry (DSC)
- Electron-Backscatter Diffraction (EBSD)

First-Principles Calculations: Motivation

- Assist the alloy design of a creep-resistant ferritic superalloy for steam-turbine applications with service temperatures up to 760°C

- Search for slow diffusers in the α-Fe matrix by first-principles calculations

- Develop the reliable kinetic database in the bcc Fe

Experimental Database

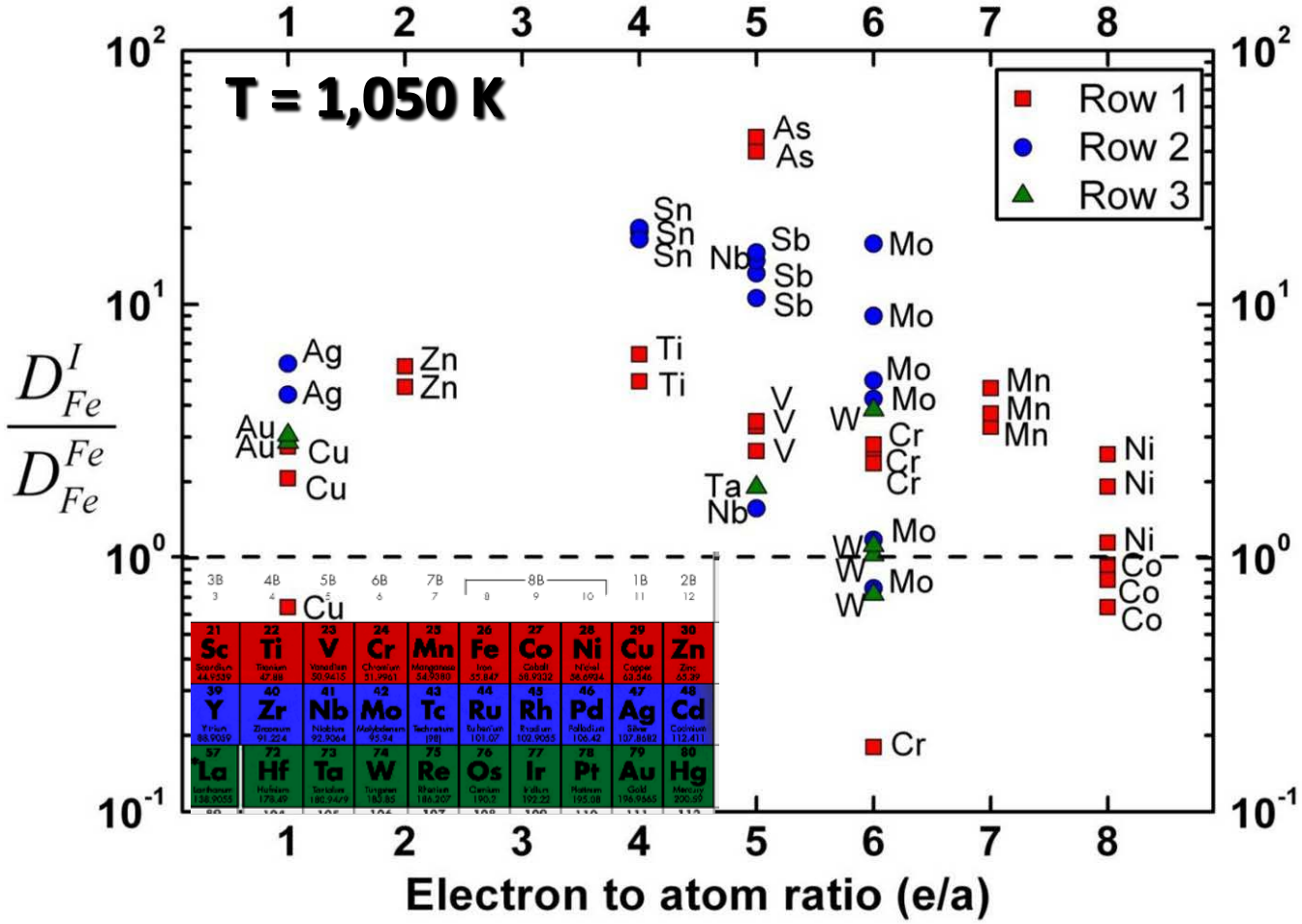

- Wide variation for several solutes (e.g., Mo and Cr)
- Experimental measurements lacking for most 5d elements
- Absence of apparent slow diffusers

Diffusion Model

Vacancy Mechanism

Vacancy Formation + Vacancy Migration

$$D = a_0^2 f_0 C_v \Gamma \qquad C_v = \exp\left(\Delta S_v^f / k_B\right)\exp\left(-\Delta H_v^f / k_B T\right)$$

$$\Delta H_v^f = E(N-1) - \left[(N-1)/N\right]E(N)$$

$$\Delta S_v^f = k_B\left[\sum_{i=1}^{3(N-1)} \ln\left(k_B T / h\nu_i^{vac}\right) - \frac{N-1}{N}\sum_{i=1}^{3N} \ln\left(k_B T / h\nu_i^{bulk}\right)\right]$$

Harmonic Transition-State Theory

$$\Gamma = \left(\prod_{i=1}^{3N-3} \nu_i^{vac} \Big/ \prod_{i=1}^{3N-4} \nu_i^{sad}\right)\exp\left(-\Delta H_v^{mig,Fe} / k_B T\right)$$

a_0: lattice parameter of Fe

f_0 : correlation factor for BCC lattice, 0.712

C_v: equilibrium-vacancy concentration

ΔS_v^f : vacancy-formation entropy

ΔH_v^f : vacancy-formation enthalpy

Γ : vacancy-hopping frequency

k_B: Boltzmann constant

$E(N)$: energy of supercell containing N atoms

$E(N-1)$: energy of supercell containing N-1 atoms and a vacancy

$\Delta H_v^{mig,Fe}$: vacancy-migration enthalpy

ν_i^{bulk} : phonon frequencies in the normal configuration of a non-defected supercell

ν_i^{vac} : phonon frequencies in the normal configuration in a supercell containing one vacancy

ν_i^{sad} : phonon frequencies in the saddlepoint configuration

$$D = D_0 \exp\left\{-Q_0^F \left[\left(1+\alpha s(T)^2\right)\Big/\left(1+\alpha\right)\right]/k_B T\right\}$$

Self Diffusion in α-Fe

$$D_0 = a_0^{\,2} f_0 \exp\left(\Delta S_v^f / k_B\right) \times \left[\prod_{i=1}^{3N} \nu_i^{vac} \Big/ \prod_{i=1}^{3N-1} \nu_i^{sad}\right] \qquad Q_0^F = \Delta H_v^f + \Delta H_v^{mig,Fe}$$

Impurity Diffusion

$$D_0 = a_0^{\,2} f_2 \exp\left(\frac{\Delta S_v^f + \Delta S_b}{k_B}\right) \times \left[\prod_{i=1}^{3N-3} \nu_i^{sol,vac} \Big/ \prod_{i=1}^{3N-4} \nu_i^{sad}\right] \qquad Q_0^F = \Delta H_v^f + \Delta H_b + \Delta H_v^{mig,I}$$

$$\Delta H_b = E(N-2,1,1) - E(N-1,1,0) - E(N-1,0,1) + E(N,0,0)$$

$$\Delta S_b = k_B \left[\sum_{i=1}^{3(N-1)} \ln\left(\nu_i^{vac} / \nu_i^{vac,sol}\right) + \sum_{i=1}^{3N} \ln\left(\nu_i^{sol} / \nu_i^{bulk}\right)\right]$$

ν_i^{sol} : phonon frequencies in the normal configuration in a supercell containing one solute atom

$\nu_i^{vac,sol}$: phonon frequencies in the normal configuration in a supercell containing one nearest - neighbor solute - vacancy pair

f_2 : correlation factor of bcc Fe lattice with impurity atom

ΔS_b : vacancy-solute binding entropy

ΔH_b : vacancy-solute binding enthalpy

$E(N-i, j, k)$: total energy of a supercell containing N-(j+k) Fe atoms, j(= 0 or 1) solute atoms, and k(= 0 or 1) vacancies

Correlation Factors

- Le Claire's formalism [1]

$$t_1 = -\frac{\Gamma_2}{\Gamma_2 + 3\Gamma_3 + 3\Gamma_3' + \Gamma_3'' - \frac{\Gamma_3\Gamma_4}{\Gamma_4 + 0.512\times\Gamma_5} - \frac{2\Gamma_3'\Gamma_4'}{\Gamma_4' + 3\times 0.512\times\Gamma_0} - \frac{\Gamma_3''\Gamma_4''}{\Gamma_4'' + 7\times 0.512\times\Gamma_0}}$$

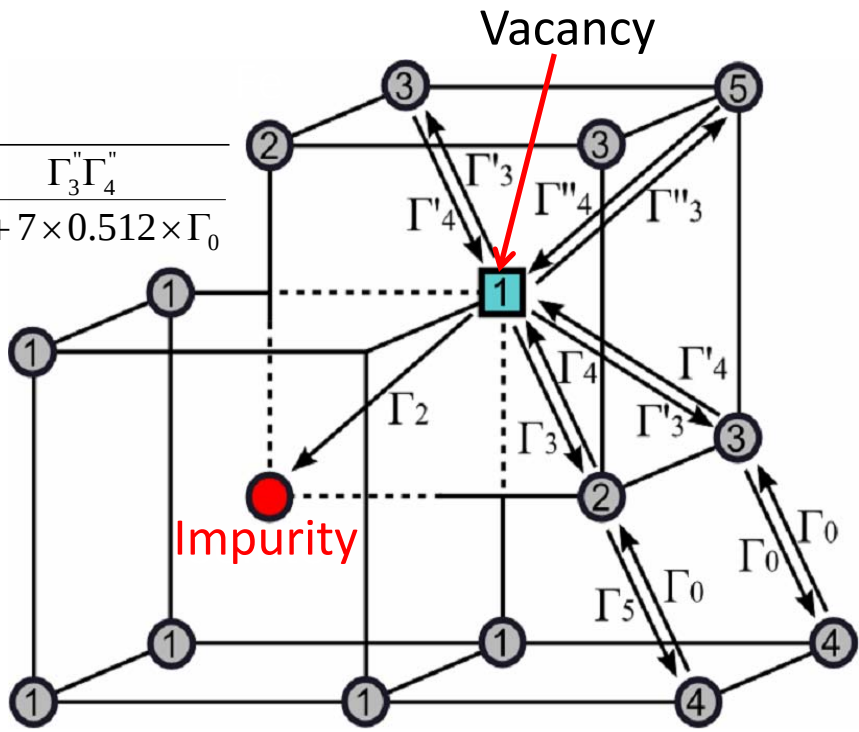

t_1: average cosine of the angles between the previous and the next jump vector, among various atomic jumps.

$$f_2 = \frac{1+t_1}{1-t_1}$$

- Input from first-principles calculations

$$\Gamma_i = \nu \exp\left(-\Delta H_i^{mig} / k_B T\right)$$

- Temperature dependencies of correlation factors are relatively weak

- The correlation factors for W and Hf are found to be very similar to those for the BCC lattice

Solute	f_{solute} / f_{Fe} @ 1,000 K
W	1.02
Mo	0.39
Zr	0.65
Hf	1.12

[1] A. D. Le Claire, In: H. Eyring, editor. Physical Chemistry: An Advanced Treatise, vol. 10, Academic Press (New York), 1970, Chap. 5.

First-principles Calculations

- Vacancy Formation, Migration, and Binding Enthalpies
  - Vienna Ab Initio Simulation Package (VASP), Projector Augmented Wave (PAW), Spin-Polarized generalized-gradient approximation (GGA)
  - 128-Atom supercells
- Entropies
  - Harmonic vibrational contributions
    - Direct force-constant approach using 54-atom supercells
  - Electronic contributions included
- Saddle-Point Geometry
  - Mid-Point between Vacancy and Solute Neighbors Assumed
  - Verified by Nudged-Elastic Band for W, Fe, and Hf

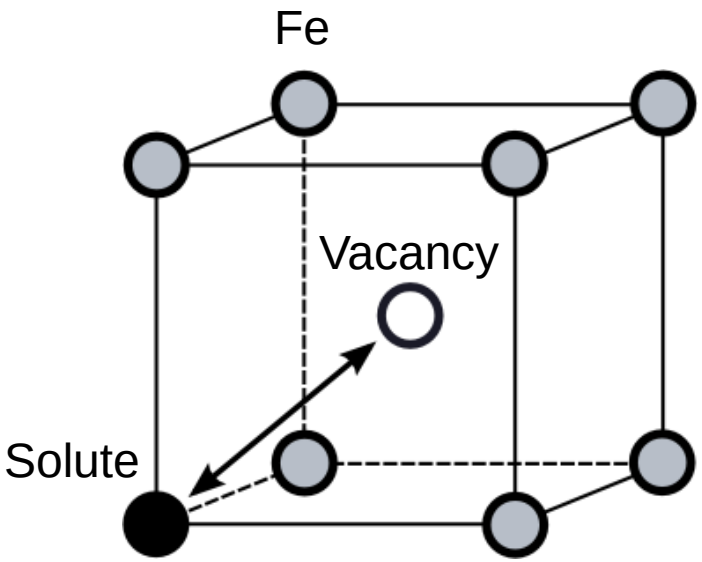

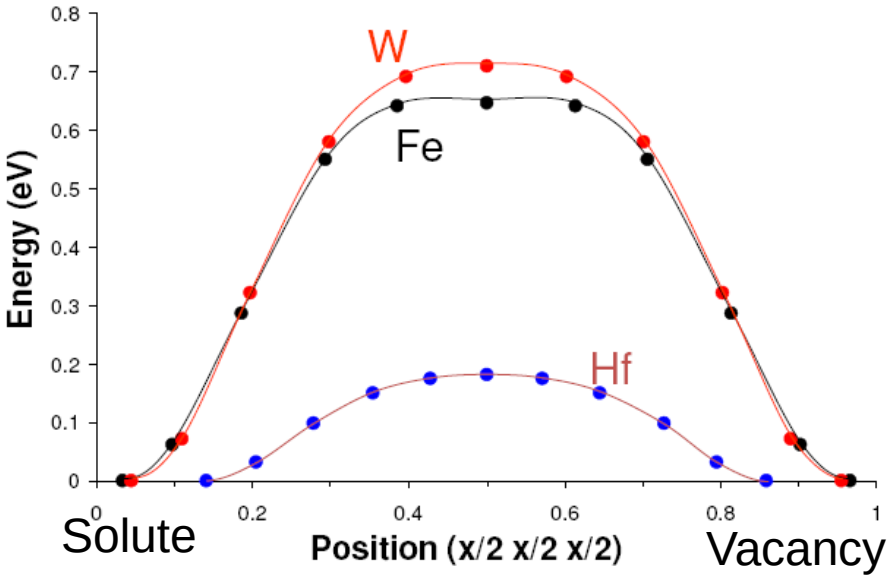

Self Diffusivities

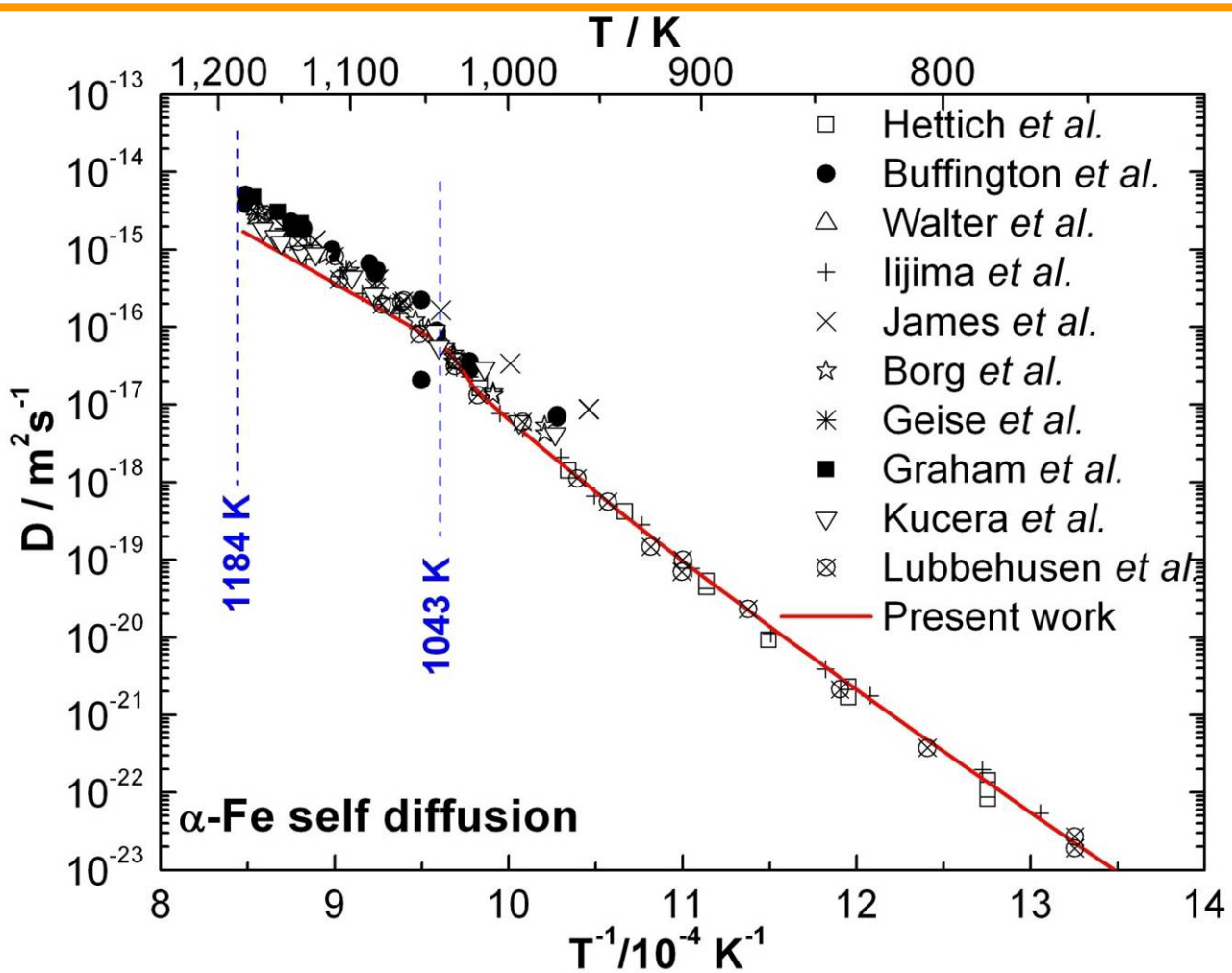

[1] R. J. Borg and C. E. Birchenall, Trans. Metall. Sot. A.I.M.E. 218, 980 (1960).
[2] F. S. Buffington, K. Hirano, and M. Cohen. Acta Metall. 9, 434 (1961).
[3] G. Hettich, H. Mehrer, and K. Maier, Scripta Metall. 11, 795 (1977).
[4] C. M. Walter and N. L. Peterson, Phys. Rer. 178, 922 (1969).
[5] D. W. James and G. M. Leak, Phil. Mag. 14, 701 (1966).
[6] Y. Iijima, K. Kimura ,and K. Hirano, Acta Met., 36, 2811 (1988).
[7] J. Geise and Ch. Herzig, Z. Metallk., 78, 291 (1987).
[8] D. Graham and D. H. Tomlin, Phil. Mag., 8, 1581 (1963).
[9] M. Lübbehusen and H. Mehrer. Acta Metall. Mater. 38, 283 (1990).
[10] J. Kucera, B. Millien, J. Ruzickova, V. Foldyna, and A. Jakobova. Acta Met. 22, 135 (1974).

Diffusivities: W

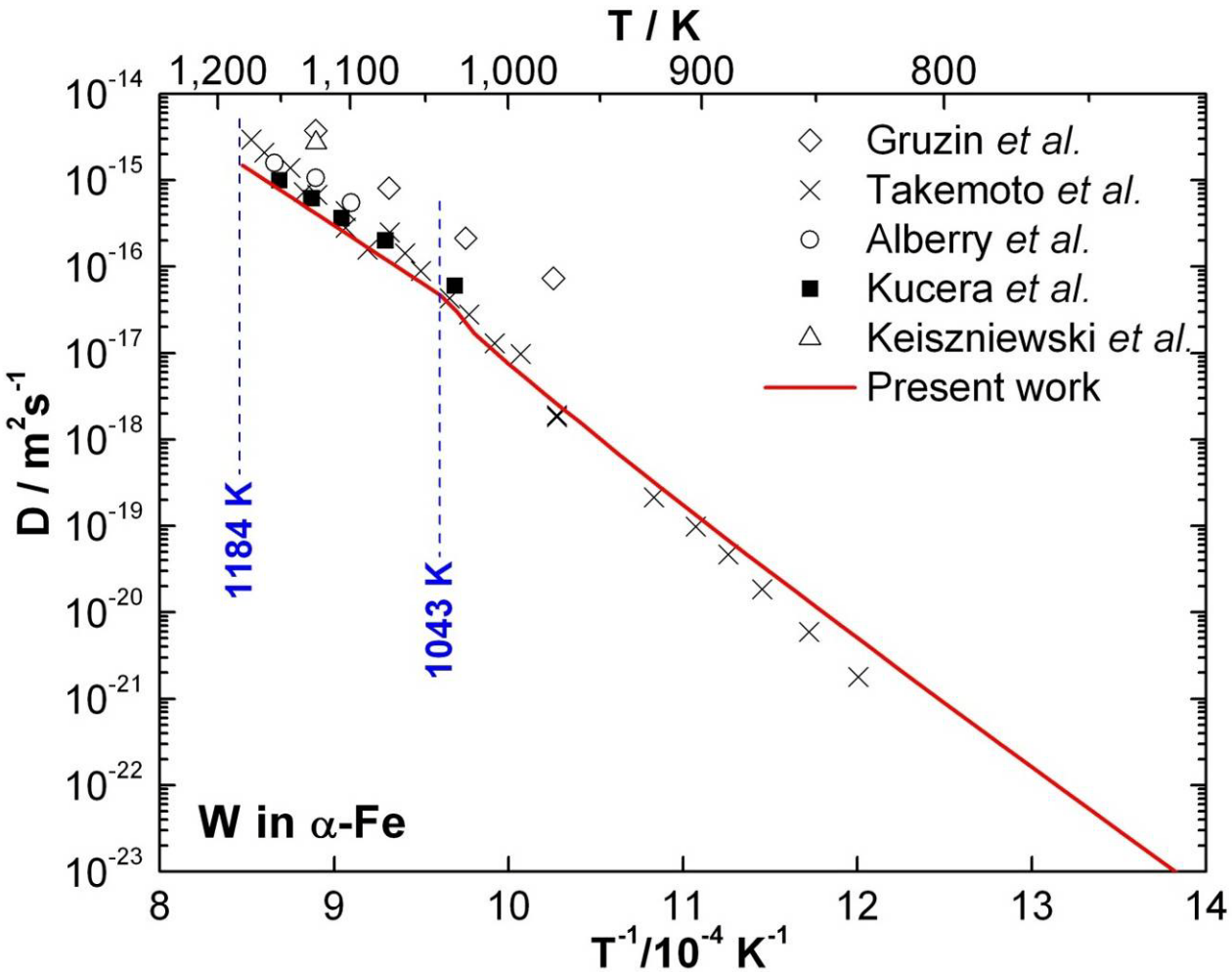

[1] P. L. Gruzin, Dokl. Akad. Nauk. SSSR 94, 681 (1954).
[2] J. Kieszniewski, Pr. Inst. Hutn. 19, 253 (1967).
[3] J. Kucera, B. Million, and K. Ciha, Kov. Mater. 7, 9 (1969).
[4] P. J. Alberry and C. W. Haworth, Met. Sci. 8, 1269 (1974).

Diffusivities: Mo

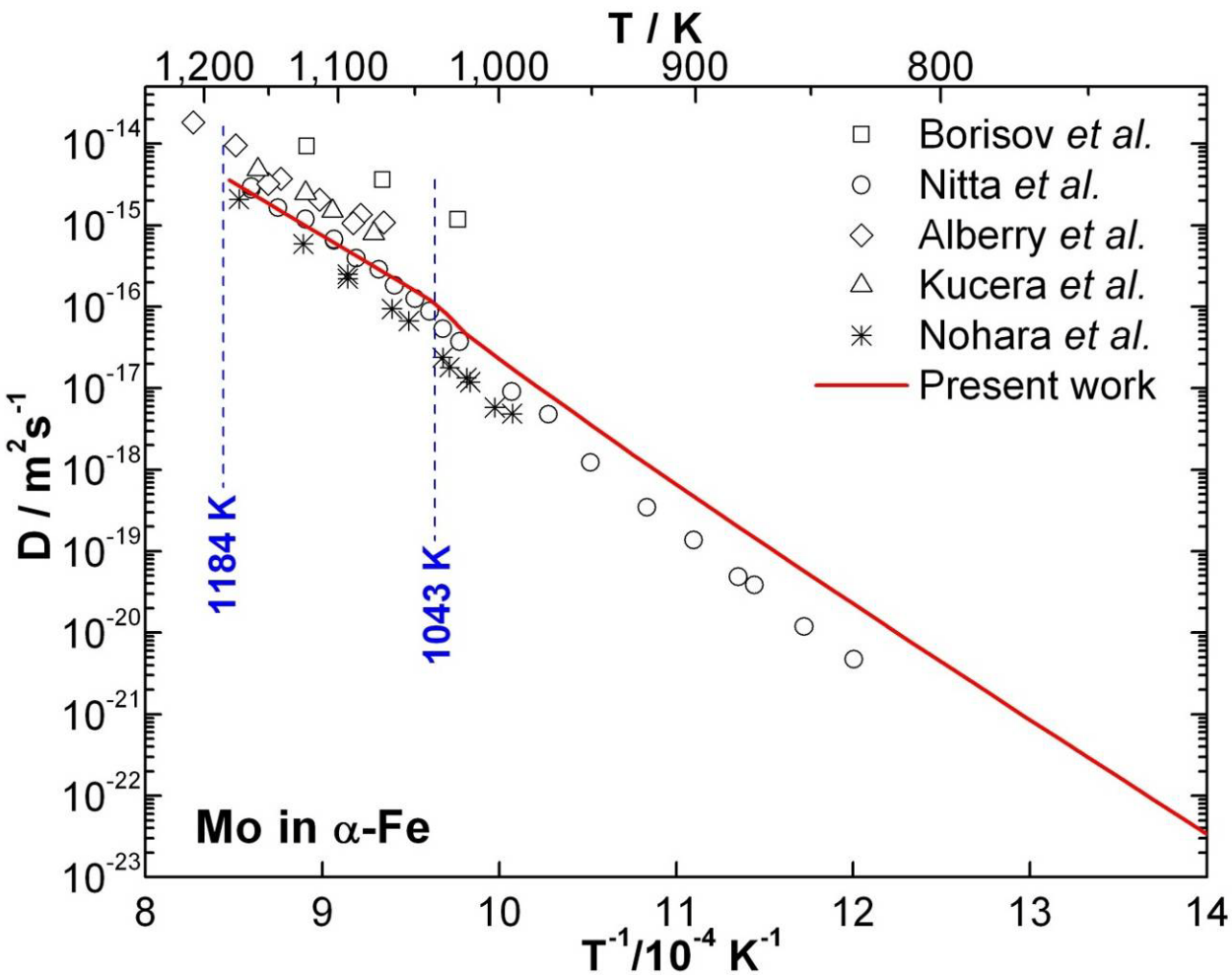

[1] V. T. Borisov, V. M. Golikov, and G. V. Sherbedinskiy, Phys. Met. Metallogr. 22, 175 (1966).
[2] J. Kucera and B. Million, and K. Ciha, Kov. Mater. 7, 97 (1969).
[3] K. Nohara and K. Hirano, J. Japan Inst. Met. 40, 407 (1976).
[4] P. J. Alberry and C. W. Haworth, Met. Sci. 8,1269 (1974).
[5] H. Nitta, Acta Materialia 50, 4117 (2002).

Compilation of Calculated Diffusivities

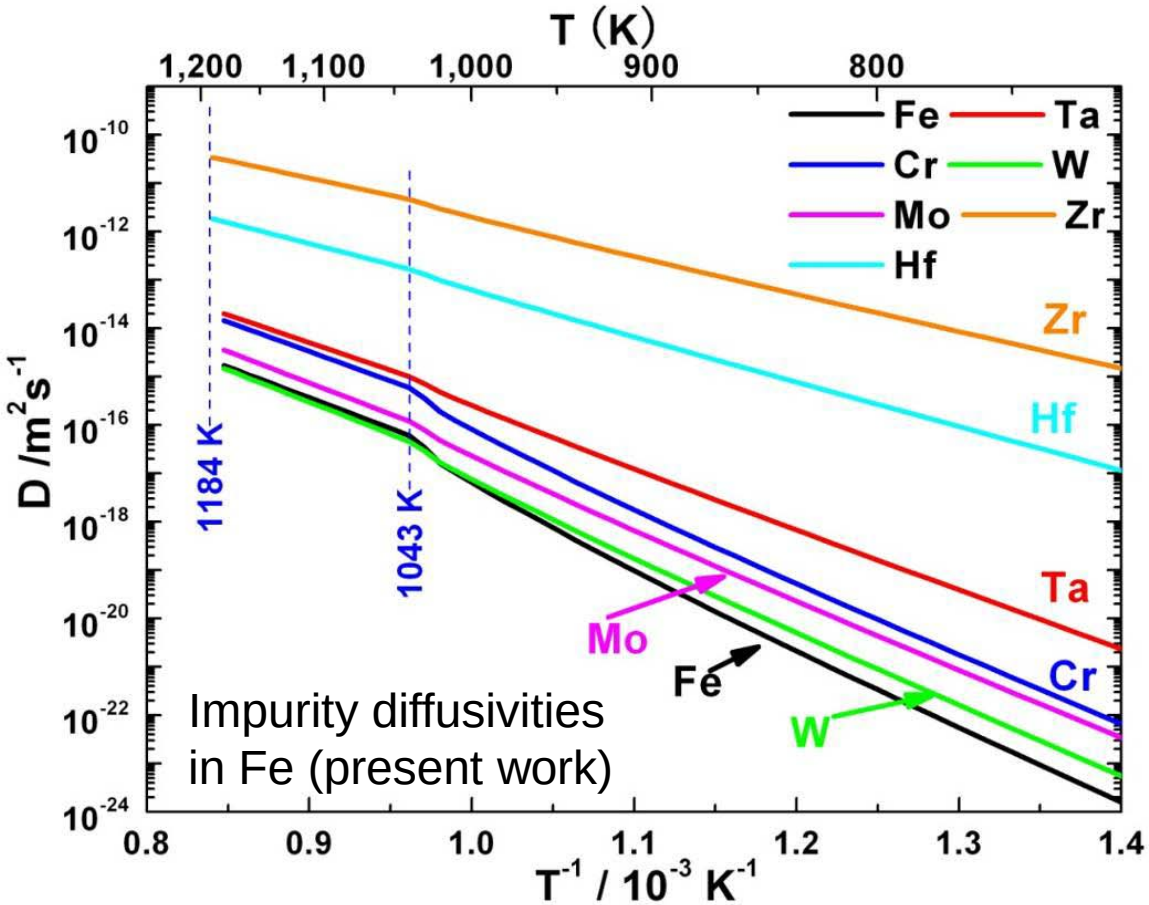

- Correlation factors for Ta and Cr are assumed to be the same as Fe.
- Solutes calculated have higher diffusivities than for Fe self diffusion, mainly due to lower activation energies.

Concentration Effect on Diffusivity

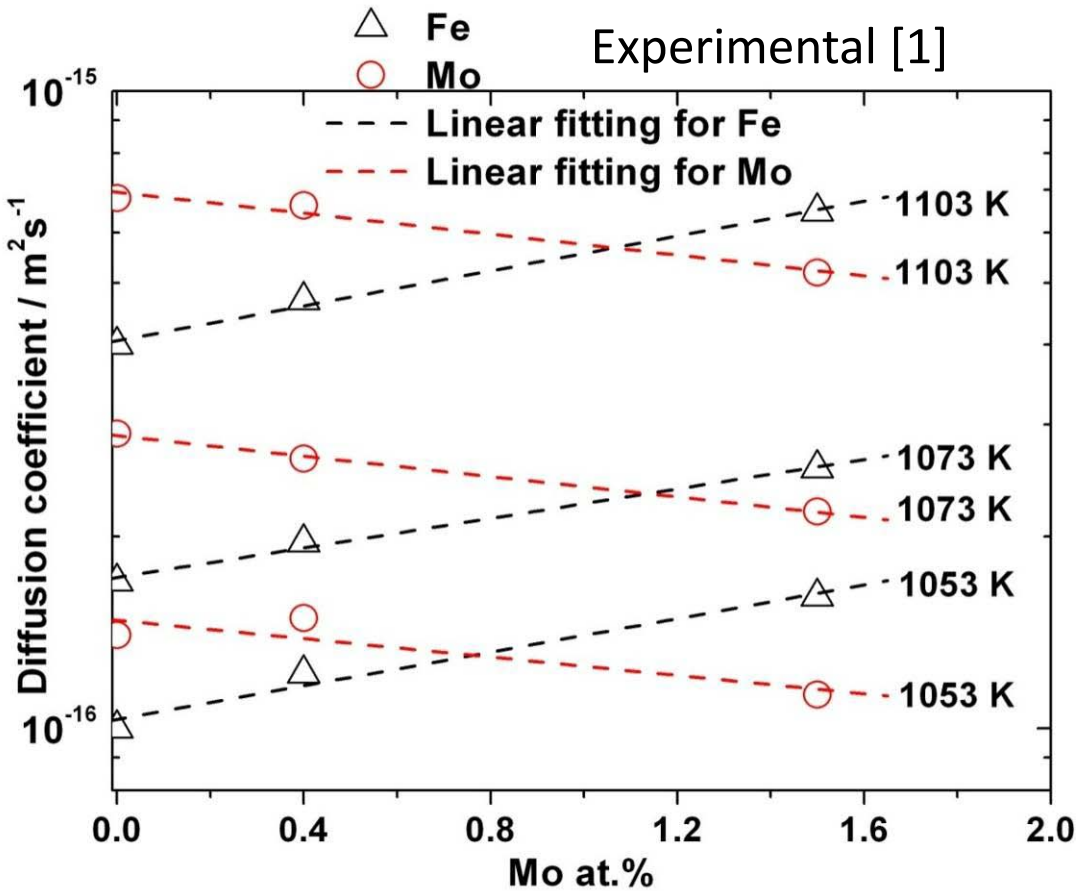

- Diffusivity of Fe is measured to increase with increasing Mo content, whereas that for Mo decreases [1]. A proper selection of Mo addition can slow the diffusion, as a guidance to the experimental alloy design.
- Future Work – to extend the current approach to study the concentration dependencies of diffusion coefficients for non-dilute Fe alloy compositions.

[1] H. Nitta, K. Miura, and Y. Iijima. Acta Mater. 54, 283 (2006).

Fabrication

- Small ingots (120 g) was vacuum arc-melted (VAR) and drop into a Cu mold with a dimension of 12.7 mm × 12.7 mm × 76.2 mm. The compositions were verified by wet chemical analyses.

- The alloy was solution-treated at 1,200℃ for 30 minutes, followed by aging at 700℃ for 100 hours.

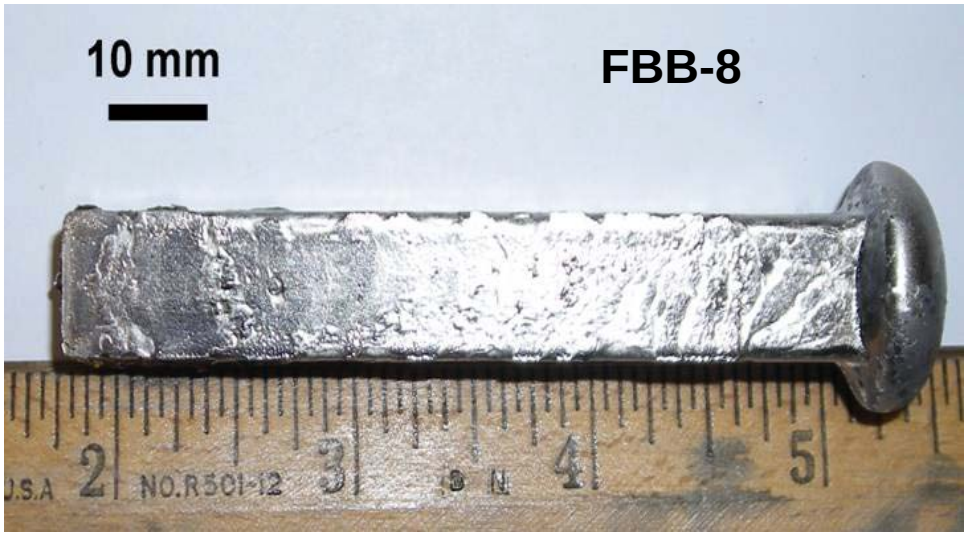

Composition (at.%)	Fe	Al	Cr	Ni	Mo
Nominal	70.1	6.5	10	10	3.4
Actual	70.28	6.45	9.97	10.02	3.28

Composition of Fe β/β' (wt.%)

Alloy	Purpose	Fe	Al	Cr	Ni	Mo	Hf	Zr	B	Nb	V	C	W	Ti
FBB-1	Based	Balance	10	10	10	-	-	-	-	-	-	-	-	-
FBB-2	Hf	Balance	10	10	10	3.4	0.25	-	0.005	-	-	-	-	-
FBB-3	Zr	Balance	10	10	10	3.4	-	0.25	0.005	-	-		-	-
FBB-4	Carbides	Balance	10	10	10	3.4	-	0.25	0.005	0.1	0.1	0.05	-	-
FBB-7	Al effect	Balance	8	10	10	3.4	-	0.25	0.005	-	-	-	-	-
FBB-8	Al effect	Balance	6.5	10	10	3.4	-	0.25	0.005	-	-	-	-	-
FBB-9	Al effect	Balance	5	10	10	3.4	-	0.25	0.005	-	-	-	-	-
FBB-12	Al effect	Balance	4	10	10	3.4	-	0.25	0.005	-	-	-	-	-
FBB-13	Al effect	Balance	3	10	10	3.4	-	0.25	0.005	-	-	-	-	-
FBB-17	Al effect	Balance	6	10	10	3.4	-	0.25	0.005	-	-	-	-	-
FBB-8W1	W effect	Balance	6.3	9.7	9.7	-	-	0.23	0.005	-	-	-	6.3	-
FBB-8W2	W effect	Balance	6.4	9.8	9.8	1.7	-	0.24	0.005	-	-	-	3.2	-
FBB-10	Mo effect	Balance	6.5	10	10	2.0	-	0.25	0.005	-	-	-	-	-
FBB-11	Mo effect	Balance	5.0	10	10	2.0	-	0.25	0.005	-	-	-	-	-
FBB-18	β' fraction	Balance	6.5	10	15	3.4	-	0.25	0.005	-	-	-	-	-
FBB-19	β' fraction	Balance	6.5	10	20	3.4	-	0.25	0.005	-	-	-	-	-
FBB-21	β' fraction	Balance	5.6	9.7	14.8	3.6	-	0.25	0.005	-	-	-	-	-

Schematic Diagram of USAXS

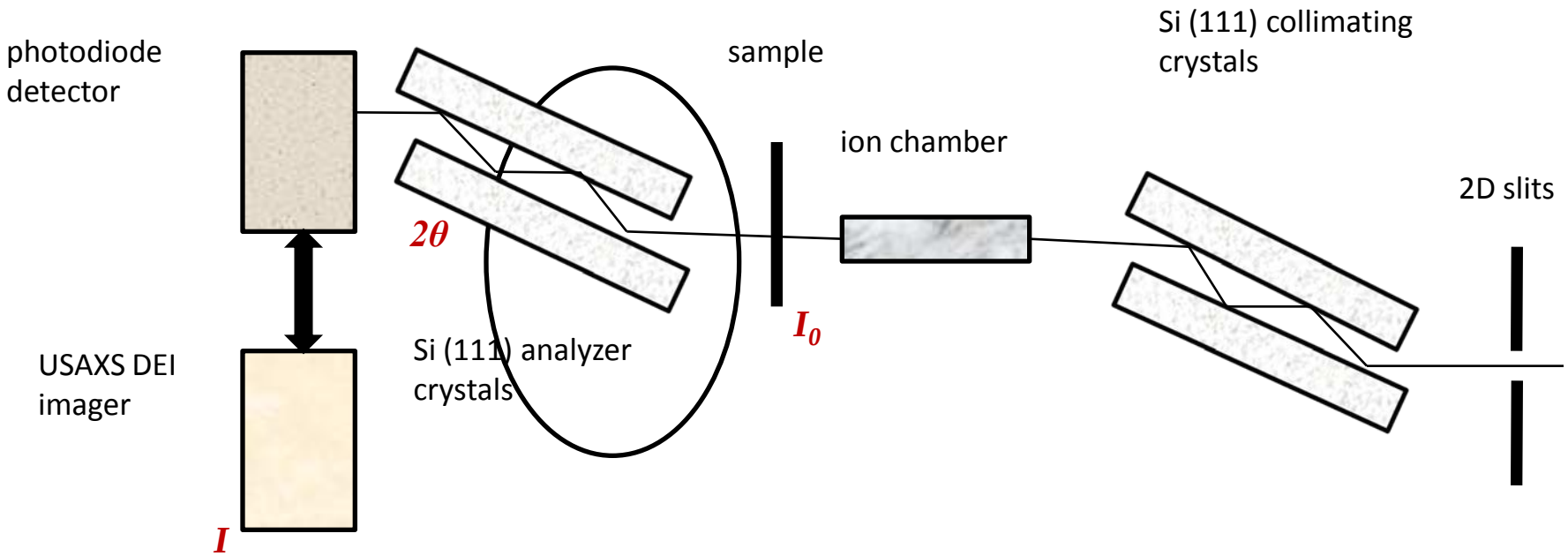

1-D collimated USAXS camera at Advanced Photon Source, 32-ID-B

USAXS:

- Measured Q range: 10^{-4} ~ 5 ×10^{-1}Å^{-1}
- Beam energy: 16.85 keV
- Beam size: 1.6 x 0.8 mm
- Foil thickness: ~ 50 µm

Theoretical Model for USAXS Data Analysis

Absolute intensity -- ***Fourier transformation of electron density***

Non-dilute precipitation: Polydispersity + Interference

Difference in scattering-length density between two phases

Scattering from grain boundaries

Number density of precipitates

Incoherent scattering intensity (background)

One population of precipitates

$$I(Q) = n_p |\Delta\rho|^2 P(Q) S(Q) + AQ^{-b} + I_{INC}$$

Form factor – particle size and shape

$$P(Q) = \left(\frac{4\pi}{3}\right)^2 \int F^2(Q,x) \times N(x,R,\delta) \times x^6 dx$$

$$F(Q,x) = [\sin(Qx) - Qx\cos(Qx)]/(Qx)^3$$

$$N(x,R,\delta) = \exp\left[-(x-R)^2/2\delta^2\right]/\sqrt{2\pi\delta^2}$$

Structure factor – inter-particle correlation

$$S(Q,L,\sigma) = 2\left\{\frac{1-\exp\left(-\frac{Q^2\sigma^2}{4}\right)\cos(QL)}{1-2\exp\left(-\frac{Q^2\sigma^2}{4}\right)\cos(QL)+\exp\left(-\frac{Q^2\sigma^2}{2}\right)}\right\}-1$$

Non-linear least-squares fitting for 8 parameters: $n_p|\Delta\rho|^2$, I_{INC}, A, R, δ, L, σ, b

USAXS Interpretations vs. TEM Results

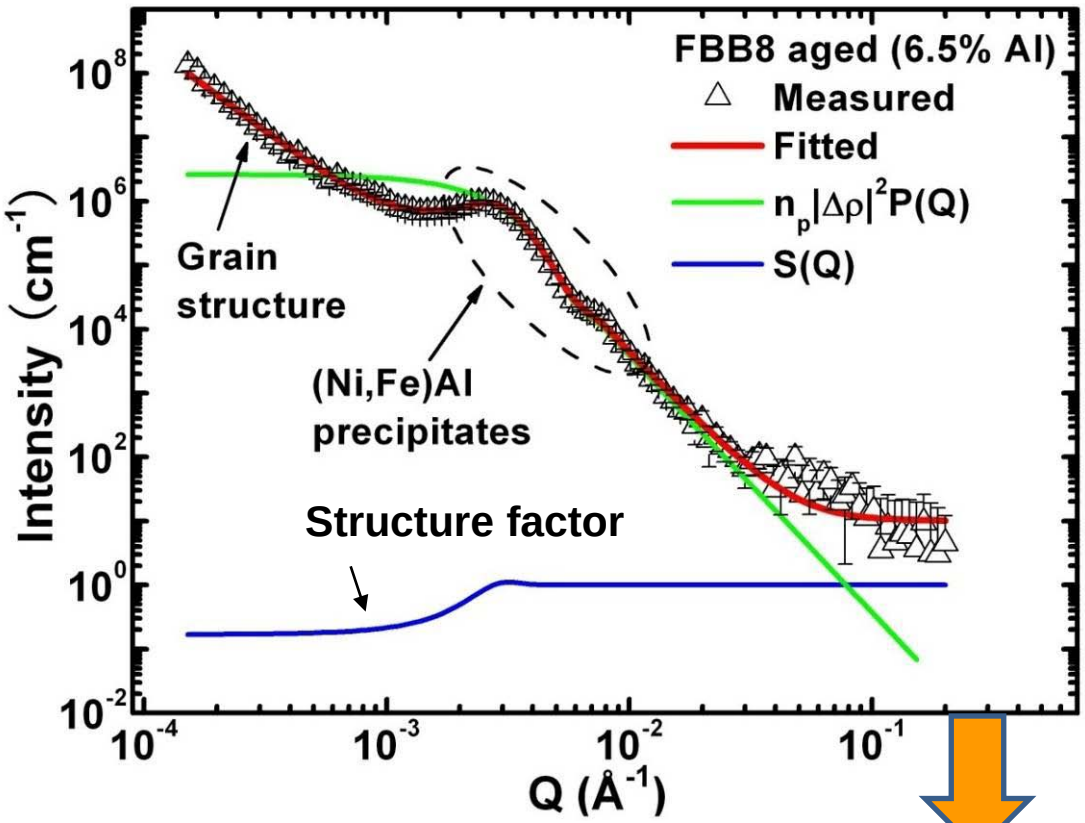

Dark-Field Image by 100_{B2} reflection

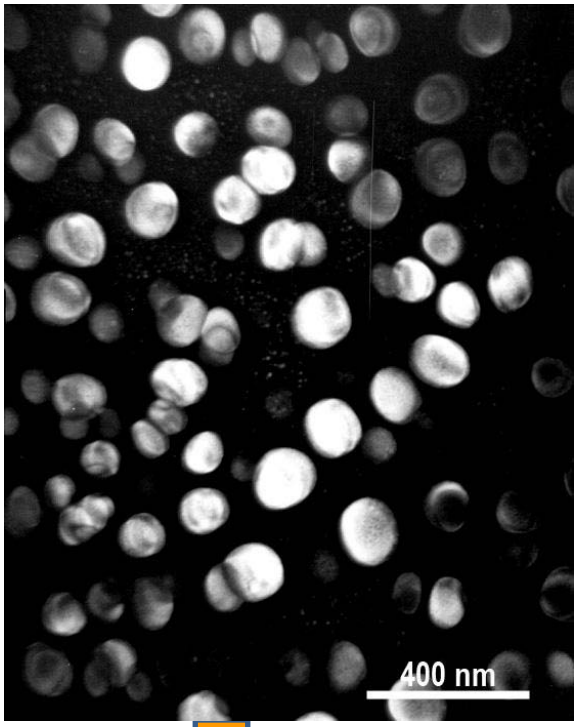

Parameters	USAXS	TEM
Diameter of precipitates (2R)	129.8 nm	130 nm
Standard deviation of diameter (2δ)	30.0 nm	25 nm
Inter-particle spacing (L)	175.0 nm	211 nm
Standard deviation of spacing (σ)	101.7 nm	37.5 nm

Schematic Diagram of APT

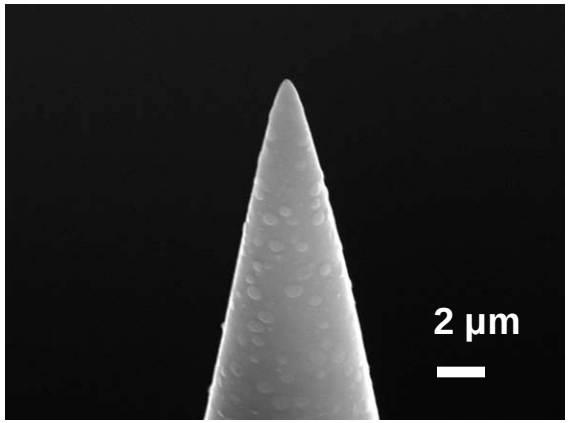

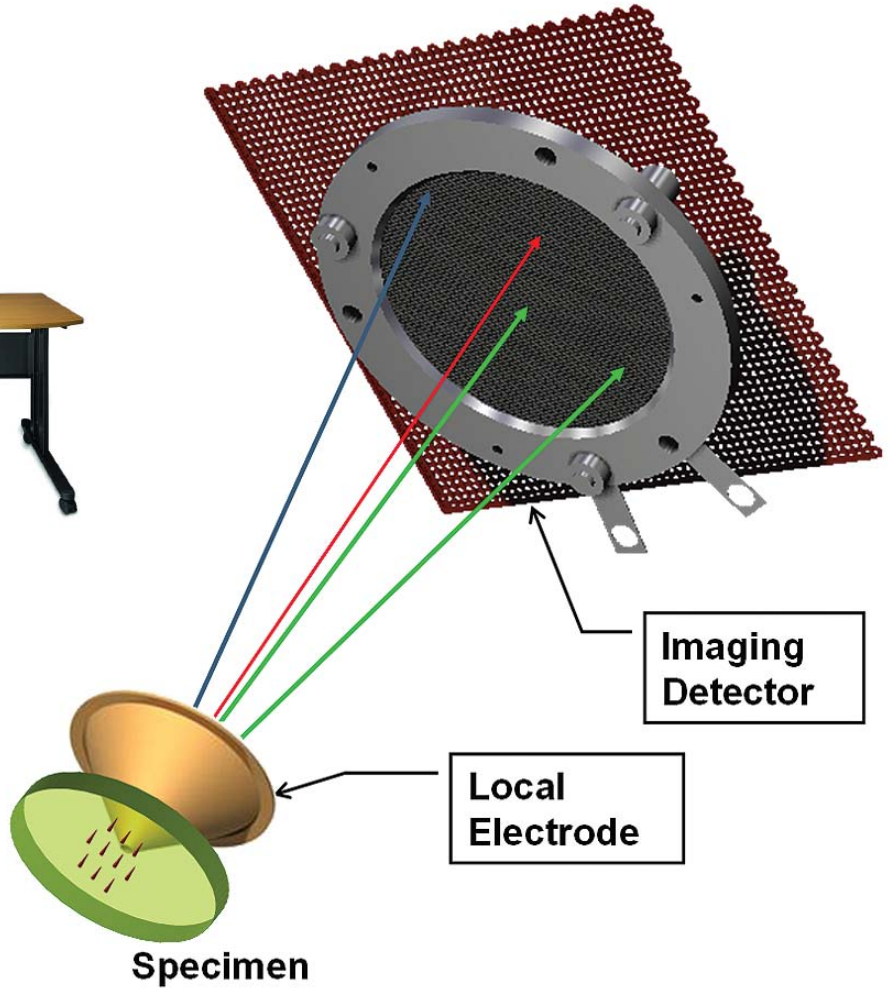

D. J. Larson and T. F. Kelly, Imago Scientific Instruments Corporation, Madison, WI, USA

Primary and Secondary Precipitates

FBB-8 (6.5Al)

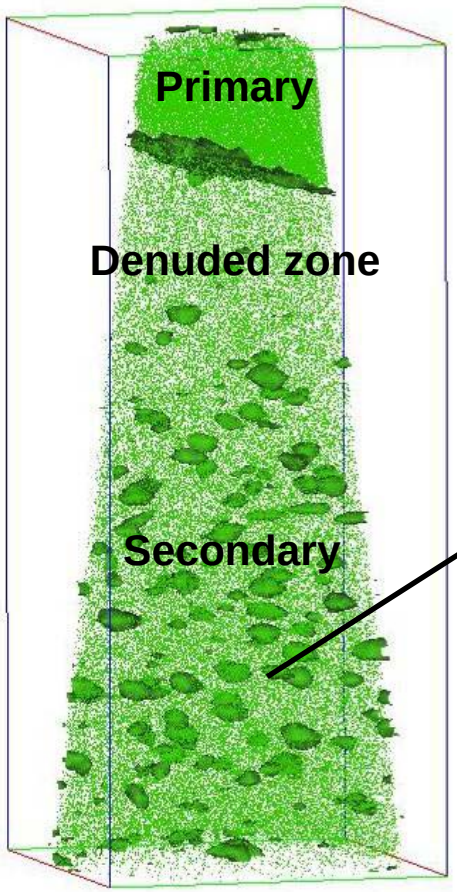

15 at.% Al iso-concentration surface

10 nm

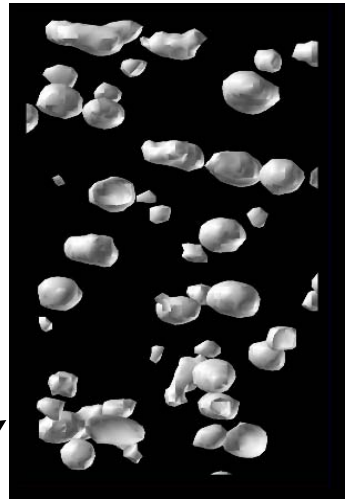

Morphology of secondary precipitates

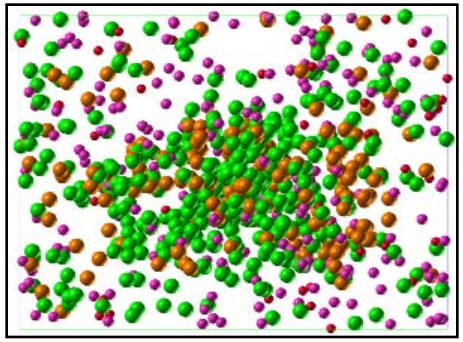

Al
Ni
Mo
Cr

2 nm

Atom map of a selected secondary precipitate

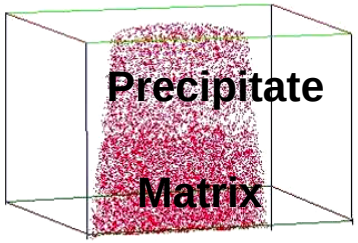

Mo-atom map

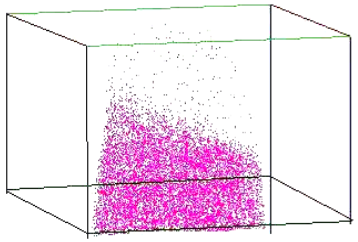

Cr-atom map

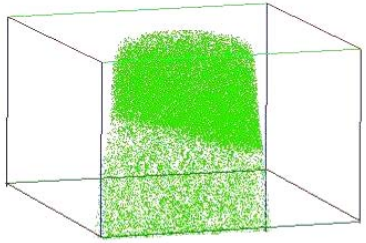

Al-atom map

Concentration Profiles

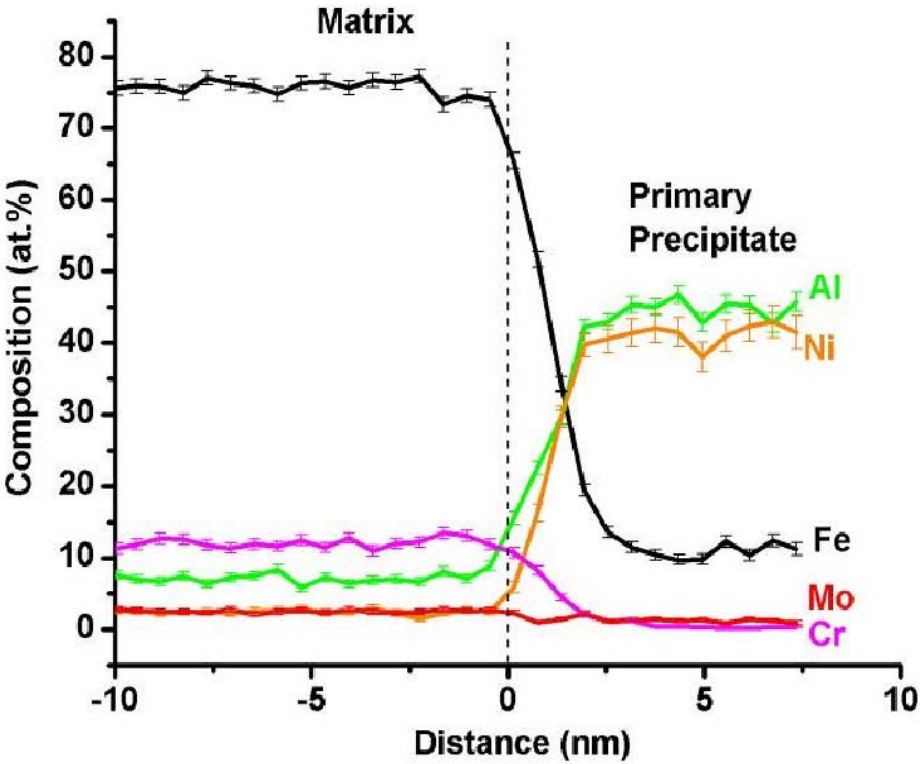

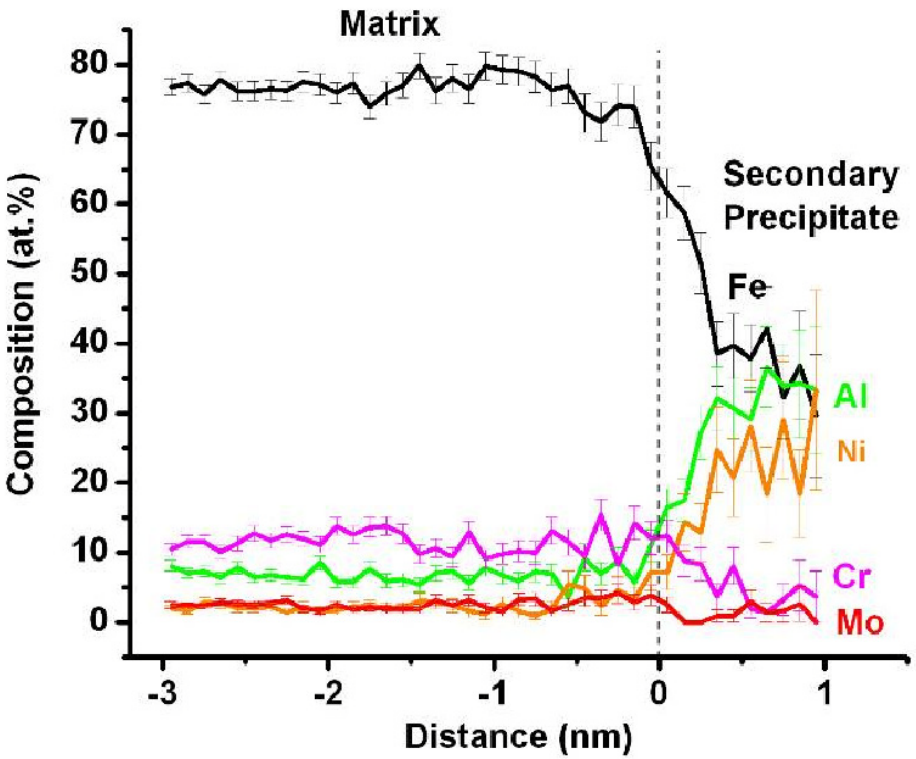

APT revealed duplex precipitation of NiAl particles: primary with an diameter of 130 nm ($Ni_{41.2}Al_{43.6}Fe_{12.7}Cr_{0.8}Mo_{1.4}$) and secondary with an diameter of 3 nm ($Ni_{26.3}Al_{41.6}Fe_{26.9}Cr_{3.3}Mo_{1.7}$).

Creep Behavior

- **Design of a series of alloys with comparable or superior creep resistance than the other ferrite-based candidate materials for steam-turbine applications.**

FBB-8: Fe-10Al-10Cr-10Ni-3.4Mo-0.25Zr-0.005B (wt.%)
FBB-21: Fe-5.6Al-9.7Cr-14.8Ni-3.6Mo-0.25Zr-0.005B (wt.%)
FBB-18: Fe-10Al-10Cr-15Ni-3.4Mo-0.25Zr-0.005B (wt.%)

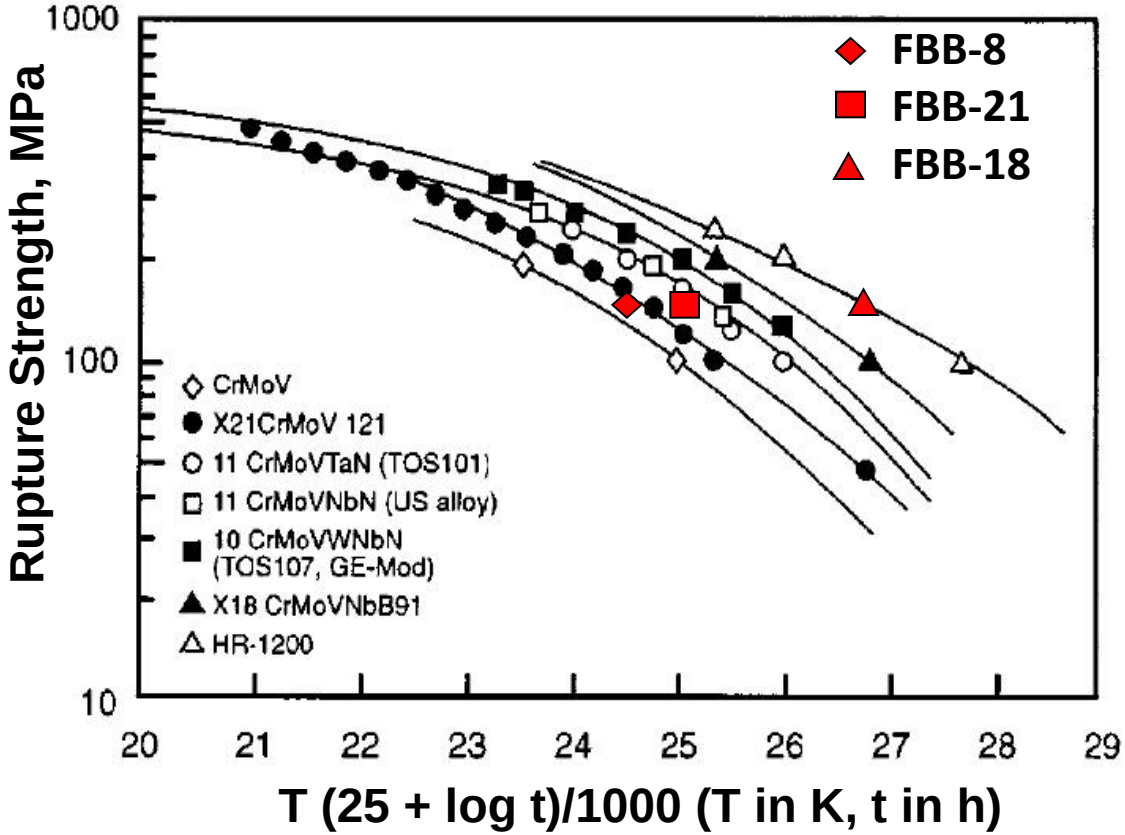

Creep Behavior: Effects of W

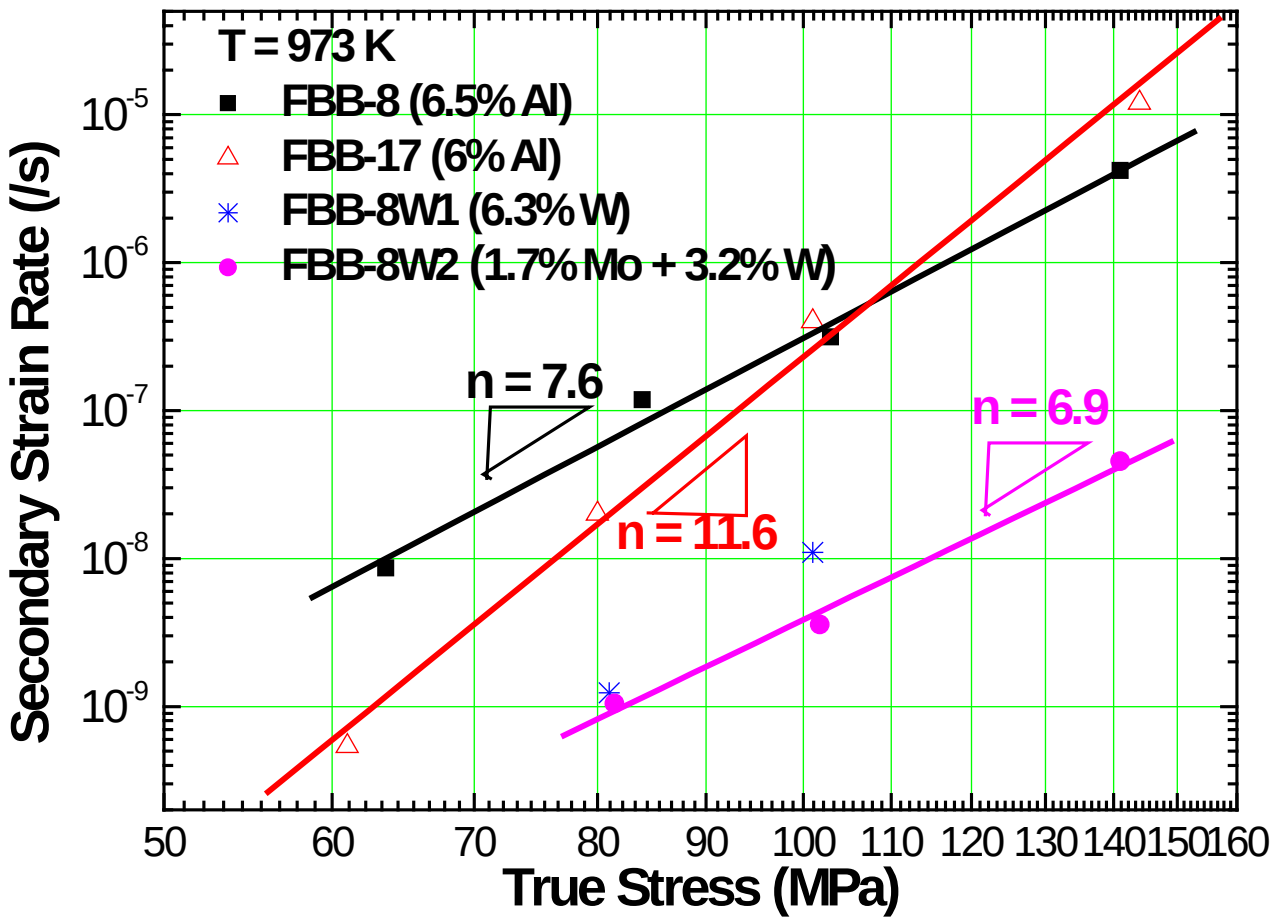

- Single slope behavior with very high apparent stress exponents
- Reduction of strain rates with addition of W
- Almost the same stress exponents with additions of Mo and W

Ductility: Unrolled Material

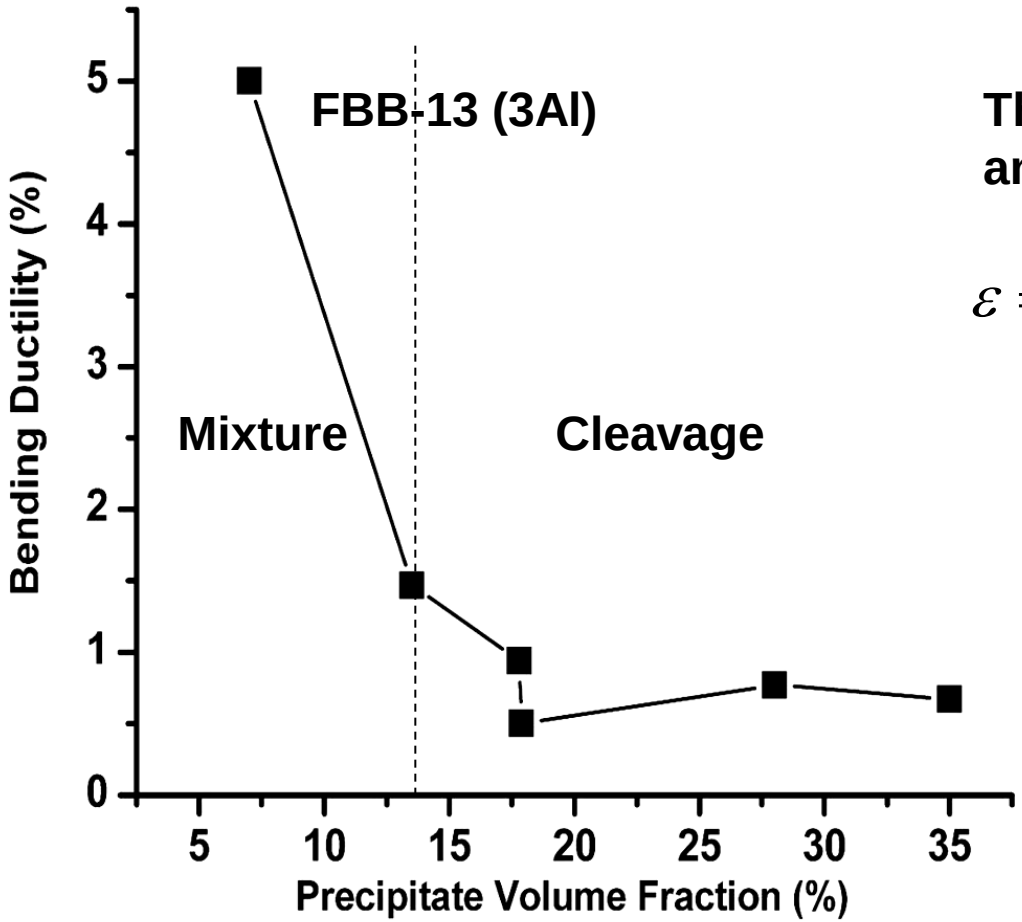

The relationship between ductility and V_{B2} can be expressed as:

$$\varepsilon = \frac{1}{C}\ln\left(\sqrt{\left(\pi / 6V_{B2}\right)} - \sqrt{2/3} + \varepsilon_n\right)$$

ε: ductility,

V_{B2}: precipitate volume fraction,

ε_n: void nucleation strain.

Brown LM, Embury JF. The microstructure and design of alloys: proceedings of the third international conference on the strength of metals and alloys 1973; 1:164.

Bending ductility reaches 5% when the precipitate volume fraction is lowered to 7%.

Ductility: Hot-rolled Material

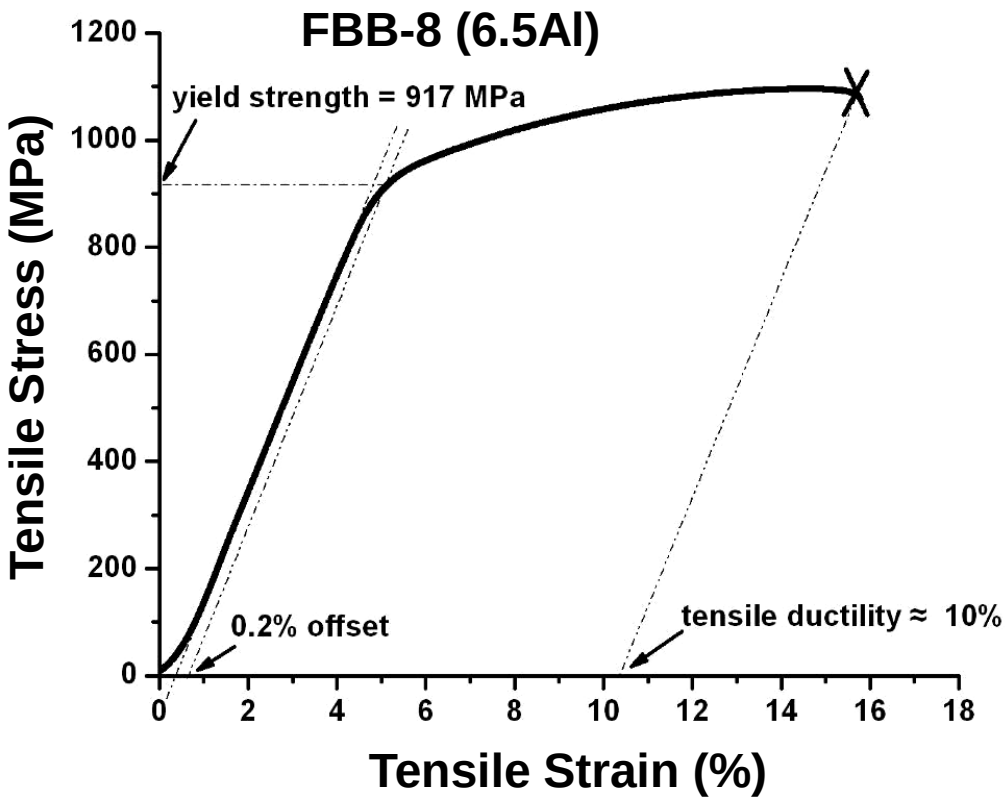

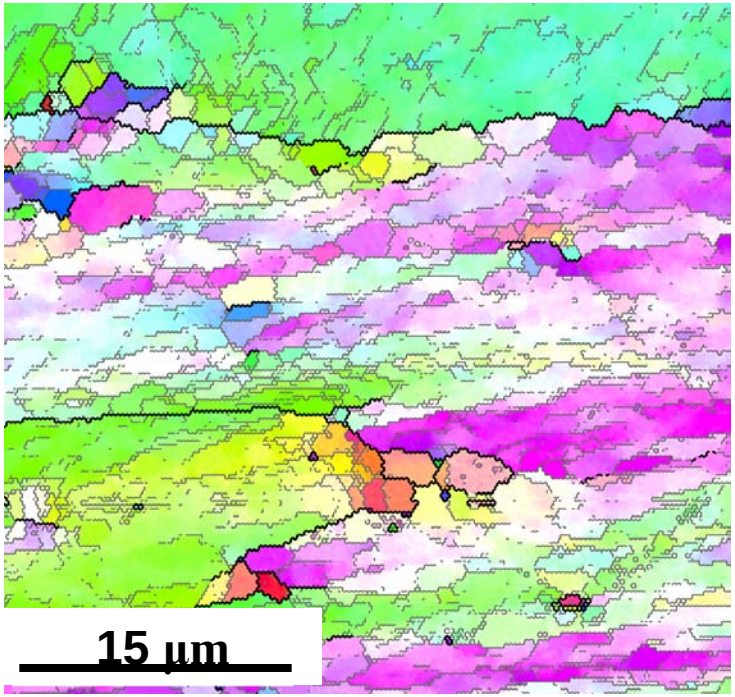

EBSD map

Tensile ductility is ~ 10% after hot rolling 80% at 750°C and the main factor contributing to the ductility improvement is the formation of subgrains with a size of about 1 µm.

Conclusions

- **First-principles calculations of diffusivities compare favorably with experiments for Fe, W, and Mo at high temperatures. Calculations are being refined to check convergence of the vibrational entropy. Search for slow diffusers continues…**

- **The designed alloy shows duplex precipitation of NiAl particles: primary with an average diameter of 130 nm and secondary with an average diameter of 3 nm. Based on APT, the primary and secondary precipitates have compositions of $Ni_{41.2}Al_{43.6}Fe_{12.7}Cr_{0.8}Mo_{1.4}$ and $Ni_{26.3}Al_{41.6}Fe_{26.9}Cr_{3.3}Mo_{1.7}$, respectively.**

- **A series of alloys with comparable or superior creep resistance relative to the other ferrite-based candidate materials, for steam-turbine applications were developed. Addition of W can significantly reduce the secondary creep rates.**

- **Grain-size refinement and precipitate-volume-fraction reduction are effective approaches to improve the ductility of the NiAl-strengthened alloys at room temperature.**

Publications

[1] S. Huang, D. L. Worthington, M. Asta, V. Ozolins, G. Ghosh, P. K. Liaw, "Calculation of impurity diffusivities in α-Fe using first-principles methods", Acta Mater., 2010;58:1982.

[2] Z. K. Teng, M. K. Miller, G. Ghosh, C. T. Liu, S. Huang, K. F. Russell, M. E. Fine, P. K. Liaw, "Characterization of nanoscale NiAl-type precipitates in a ferritic steel by electron microscopy and atom probe tomography", Scripta Mater., 2010;63:61.

[3] Z. K. Teng, C. T. Liu, G. Ghosh, P. K. Liaw, M. E. Fine, "Effects of Al on the microstructure and ductility of NiAl-strengthened ferritic steels at room temperature", Intermetallics, 2010, in press.

[4] Z. K. Teng, C. T. Liu, M. K. Miller, G. Ghosh, E. Kenik, S. Huang, P. K. Liaw, "Room temperature ductility of NiAl-strengthened ferritic steels: effects of precipitate microstructure and hot rolling", 2010, in preparation.

[5] Z. K. Teng, F. Zhang, M. K. Miller, S. Huang, Y. T. Chou, R. H. Tien, C. T. Liu, Y. A. Chang, P. K. Liaw, "Development of new ferritic steels with combined optimum creep resistance and ductility by coupling thermodynamic calculations with focused experiments", 2010, in preparation.

[6] S. Huang, X. Li, G. Ghosh, E. A. Kenik, J. Ilavsky, Z. Teng, G. Wang, M. E. Fine, C. T. Liu, L. Liu, P. K. Liaw, "Study of the nanoscale (Ni,Fe)Al precipitates in the ferritic superalloy by ultra-small-angle X-ray scattering", 2010, in preparation.

[7] S. Huang, E. A. Kenik, J. Ilavsky, G. Ghosh, Z. Teng, G. Wang, M. E. Fine, C. T. Liu, P. K. Liaw, "Effects of Al on the creep behavior and microstructure of a ferritic superalloy strengthened by NiAl precipitates", 2010, in preparation.

Presentations

[1] P. K. Liaw, C. T. Liu, G. Ghosh, M. E. Fine, M. Asta, M. K. Miller, S. Huang, Z. K. Teng, G. Y. Wang, "Computational design and prototype evaluation of aluminide-strengthened ferritic superalloys for power-generating turbine applications up to 1,033 K," International Conference on Advanced High-Temperature and High-Strength Structural Materials (HTHSSM), Hong Kong, Oct. 4-8, 2009.

[2] S. Huang, D. L. Worthington, M. Asta, V. Ozolins, G. Ghosh, P. K. Liaw, "First-principles calculation on impurity diffusivities in ferritic iron", The TMS 138th Annual Meeting & Exhibition, San Francisco, CA, Feb. 15-19, 2009.

[3] Z. K. Teng, P. K. Liaw, C. T. Liu, G. Ghosh, M. E. Fine, S. Y. Huang, G. Y. Wang, "Ductility of NiAl-strengthened ferritic superalloys at room temperature," The TMS 138th Annual Meeting & Exhibition, San Francisco, CA, Feb. 15-19, 2009.

[4] Z. K. Teng, C. T. Liu, M. K. Miller, G. Ghosh, E. Kenik, S. Huang, P. K. Liaw, "Room temperature ductility of NiAl-strengthened ferritic steels: effects of precipitate microstructure and hot rolling", The TMS 139th Annual Meeting & Exhibition, Seattle, WA, Feb.14-18, 2010.

[5] S. Huang, X. Li, G. Ghosh, E. A. Kenik, J. Ilavsky, Z. K. Teng, G. Wang, M. E. Fine, C. T. Liu, L. Liu, P. K. Liaw, "Investigation of the nanoscale NiAl precipitates in the ferritic superalloy by USAXS", The TMS 139th Annual Meeting & Exhibition, February, Seattle, WA, Feb. 14-18, 2010.

[6] P. K. Liaw, S. Huang, Z. K. Teng, "Computational and Experimental Design of Ferritic Superalloys for Elevated-Temperature Applications," DOE program review meeting with Vito Cedro, Knoxville, TN, April 23, 2010.

Awards

Zhenke Teng:

[1] 1st and 2nd Place Awards, Annual Sigma Xi Student Presentation Competition, University of Tennessee, Knoxville, April 16, 2009 and March 23, 2010.

[2] 1st Place Award, Oak Ridge Chapter of the 2009 ASM International Educational Symposium Student Poster Competition, April 22, 2009.

[3] Winner of the 2010 TMS Annual Student Poster Contest in Structural Materials Division. The TMS 139th Annual Meeting & Exhibition, Seattle, WA, Feb. 14-18, 2010.

Shenyan Huang:

[1] 2nd and 1st Place Awards, Annual Sigma Xi Student Presentation Competition, University of Tennessee, Knoxville, April 16, 2009 and March 23, 2010.

[2] 2nd Place Award, Student Research Poster Presentation, Oak Ridge Chapter of ASM International, November 19, 2009.

[3] 3rd Place Award, Oak Ridge Chapter of the 2009 ASM International Educational Symposium Student Poster Competition, April 22, 2009.

Morris E. Fine: **University of Minnesota Alumni Outstanding Achievement Award, 2010**

Peter K. Liaw: **L. R. Hesler Award 2010, University of Tennessee**

Future Work (1)

- **TEM characterizations of tensile-crept alloys interrupted during the secondary-creep regime (dislocation-particle interactions, grain-boundary structures, and other minor phases).**

- **Effects of Mo and W additions on FBB8 (6.5Al). New phase? Misfit? Partitioning? Diffusion?**

- **Evaluation of creep properties and microstructures of FBB8 aged and crept at 760°C**

- **Lattice-strain measurements during in-situ creep by neutron diffraction**

Future Work (2)

- **Search for slow diffusers by first-principles calculations continues (calculations of other candidates: Nb, Ti, etc.)**
- **First-principles calculations of Fe/B2 interfacial energies.**
- **Determination of the alloys with optimal combined ductility and creep resistance.**
- **Creep studies on the hot-rolled materials.**
- **Oxidation and corrosion investigations in a mixture of air and water vapor at 700°C and 760°C (Collaboration with Dr. Peter Tortorelli and Dr. Bruce Pint at ORNL, or Dr. Wu Kai at National Taiwan Ocean University).**

Effects of Al% and Dislocation-Particle Interactions

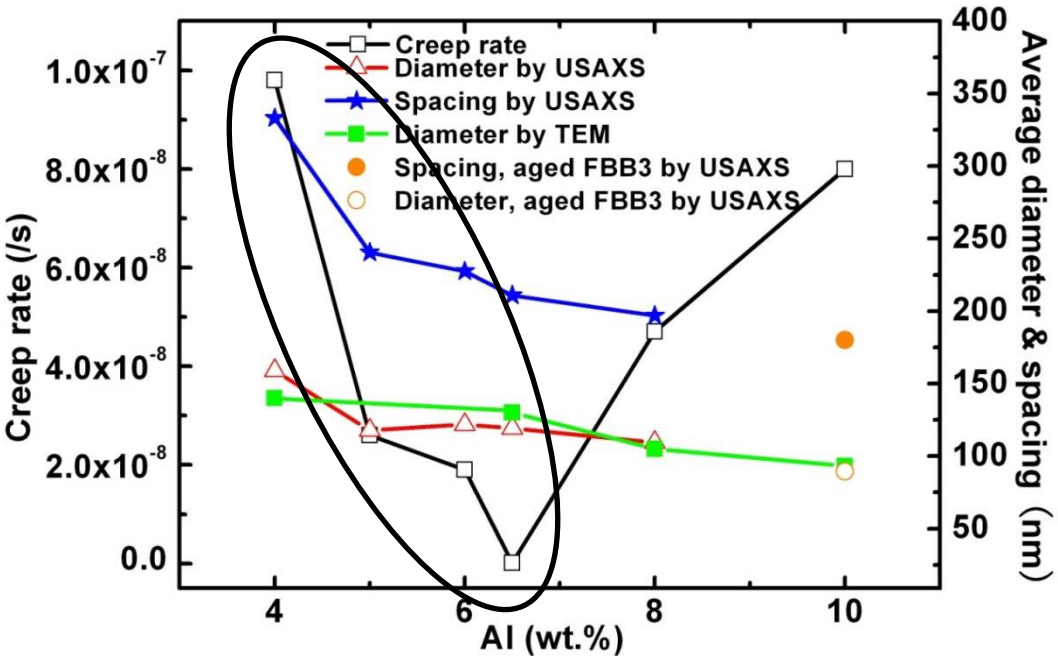

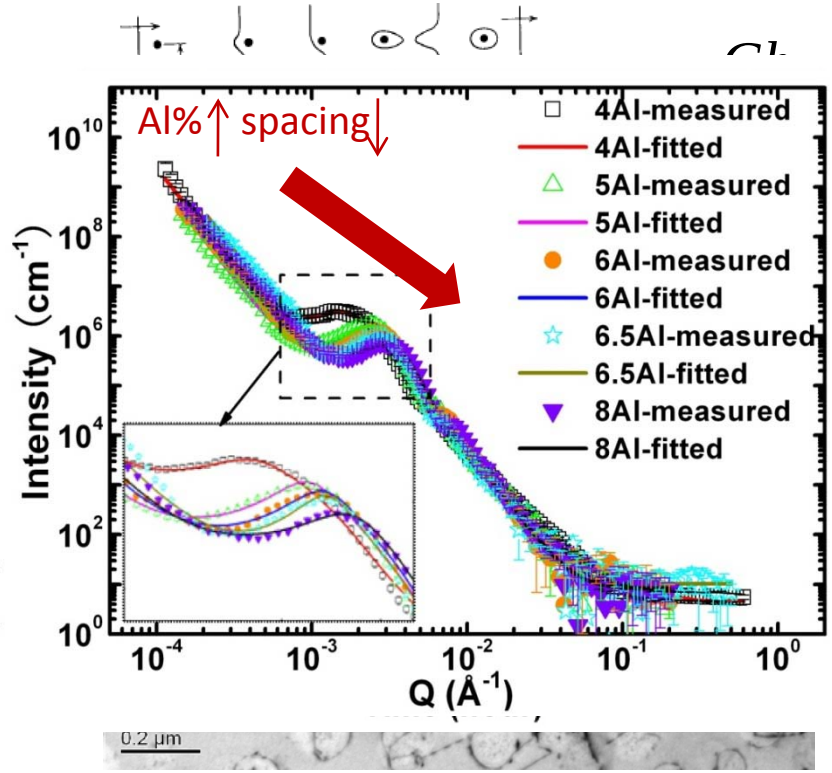

red: Orowan bowing; blue: dislocation climb

- Dramatically and slightly decreased spacing and diameter reflect that a higher volume fraction is responsible for the enhanced creep resistance. Dislocation motion is inhibited by Orowan bowing (dislocation loops) and dislocation climb mechanisms.
- However, such correlation is not valid for FBB7 (8% Al) and 3 (10% Al), indicating that precipitates are not likely to be the reason for inferior creep properties.

First-principles Calculation of Fe/B2 Interfacial Energy

- Computational Tools and Resources
  - Computational resources:
    - First-principles electronic structure code: VASP (http://cms.mpi.univie.at/vasp/vasp/)
    - Hardware: PSC SGI Altix 4700 (http://www.psc.edu/machines/sgi/altix/pople.php) and NICS Cray XT5 (http://www.nics.tennessee.edu/computing-resources/kraken)
- Computational Methodology
  - Supercell Method:
    - Supercells of different sizes are constructed with {100}, {110} and {111} habits
    - Convergence of calculated interfacial energy is checked w.r.t. supercell size
    - Calculated interfacial energy (γ) is defined as

$$\gamma = (E_{Fe/B2}[n_{Fe}, n_{B2}] - 0.5(E_{Fe}[2n_{Fe}] + E_{B2}[2n_{B2}]))/2A$$

where the supercell contains *n* unit cells of Fe (n_{Fe}) and *B2* (n_{B2}) phases, *E* is the corresponding total energy, and *A* is the interfacial area interfacial energy

First-principles Calculation of Fe/B2 Interfacial Energy

- Computational Results
  - Fe/NiAl and Fe/CoAl Interfacial Energies

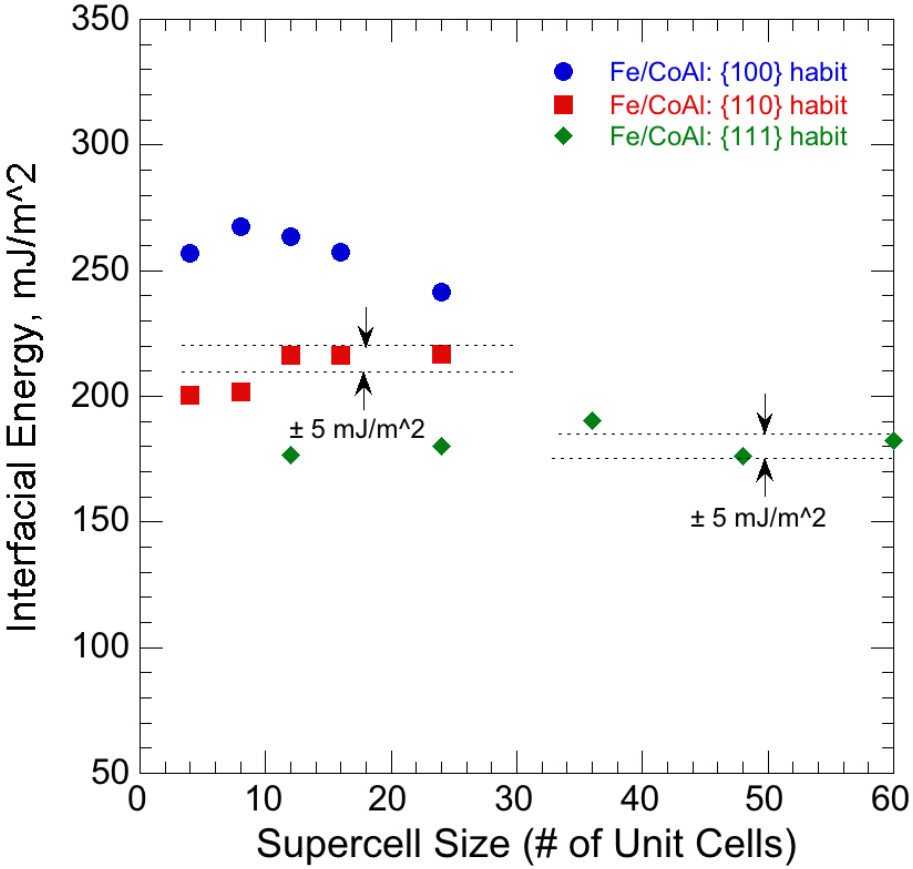

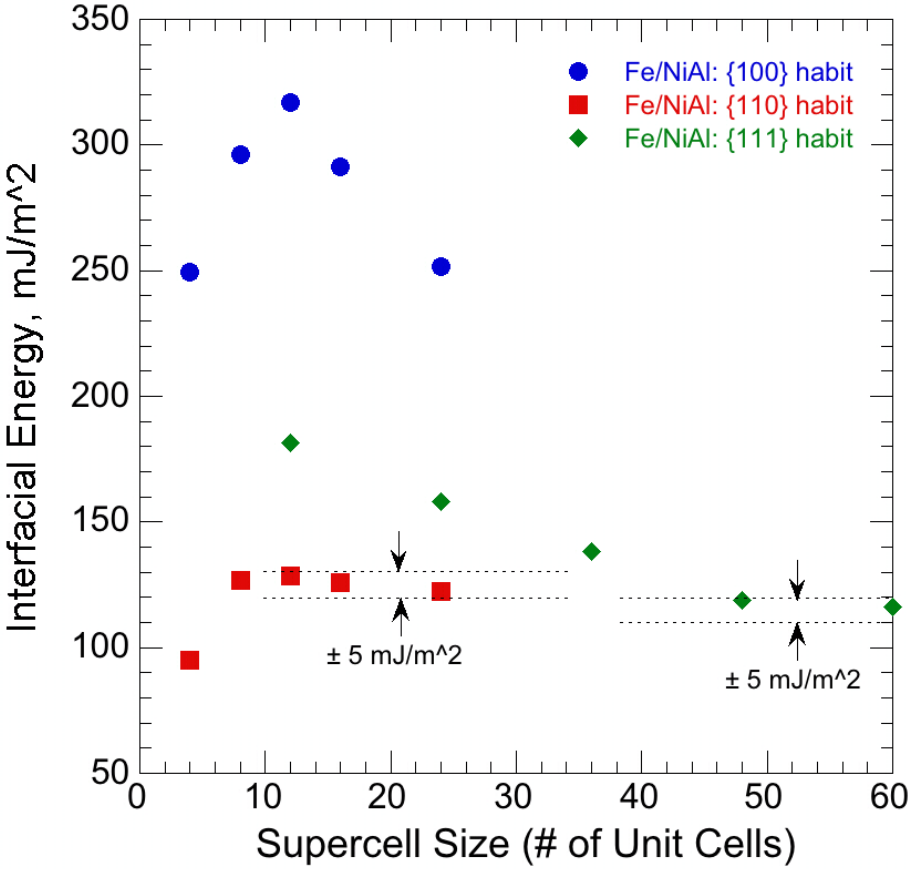

- Further Work in Progress
  - Supercell Method:
    - Calculations of Fe/FeAl interfacial energies
    - Convergence of {100} interfacial energies in all cases

Theoretical Model for USAXS Data Analysis

A: scattering amplitude for grain-boundary scattering

R: average radius of precipitates

δ: standard deviation of average radius

L: average inter-particle spacing

σ: standard deviation of average inter-particle spacing

b: fractal parameter of grain-boundary surface

To be calculated:

1) Correlation factors for solutes

2) Vacancy formation, migration, and vacancy-solute binding enthalpies

3) Electronic entropies and vibrational entropies through vibrational frequencies

Magnetic Effects on Activation Energy

$$Q^F(T) = Q^P\left(1 + s(T)^2\,\alpha\right)$$

$$Q^P = \frac{Q_0^F}{1+\alpha}$$

$$s(T) = M(T)/M(0)$$

$Q^{P(F)}$: activation energy in the paramagnetic (ferromagnetic) state

Q_0^F : activation energy at 0 K

α: a species-dependent parameter

$s(T)$: a ratio of the magnetization, M, at T and 0 K

ΔM_{12}: the induced magnetization of the impurity in the first and second neighbors

$$\alpha \propto \Delta M_{12} = \sum_{i=1}^{8} \Delta m_i^{1st\ NN} + \sum_{j=1}^{6} \Delta m_j^{2nd\ NN}$$

- α quantifies the effect of magnetization on Q in ferromagnetic phase.
- Linear empirical relation between α and induced magnetization was found.

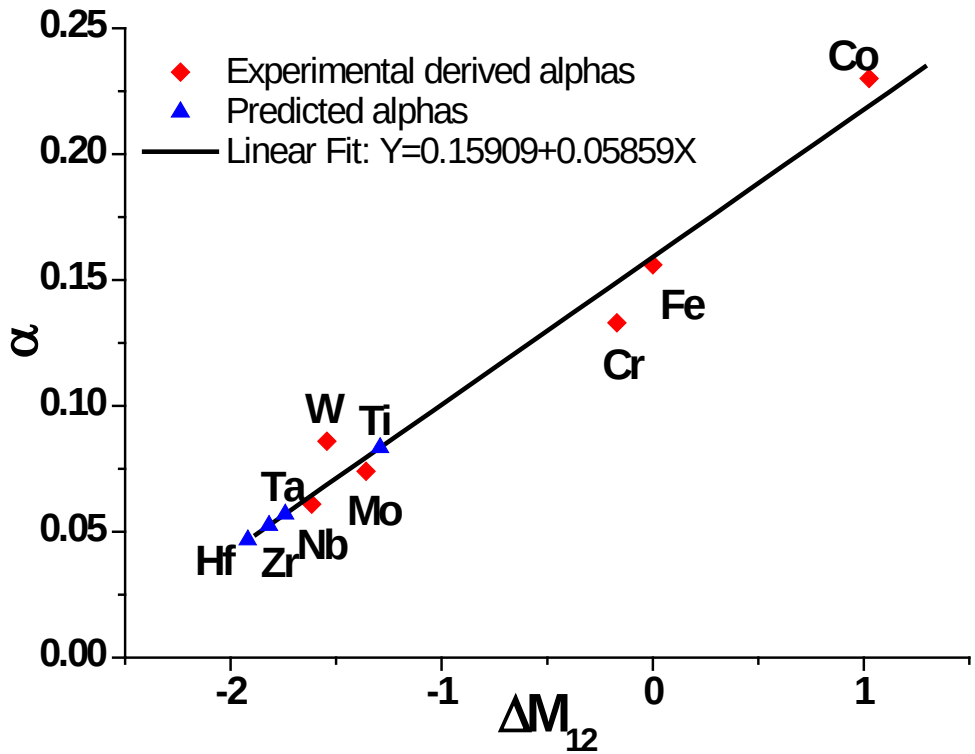

Fabrication

- Small ingots (120 g) was vacuum arc-melted (VAR) and drop into a Cu mold with a dimension of 12.7 mm × 12.7 mm × 76.2 mm. The compositions were verified by wet chemical analyses.

- The alloy was solution-treated at 1,200℃ for 30 minutes, followed by aging at 700℃ for 100 hours.

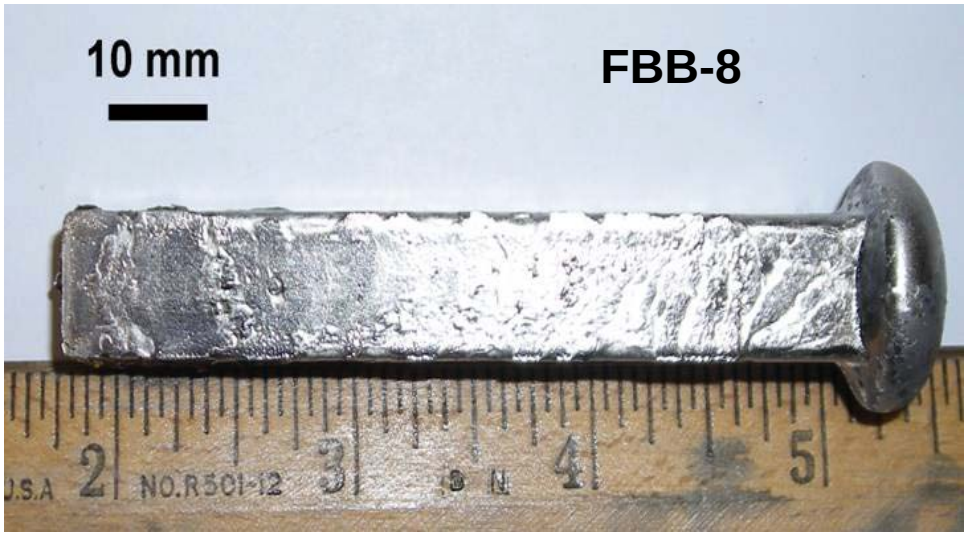

Composition (at.%)	Fe	Al	Cr	Ni	Mo
Nominal	66.1	12.7	10.2	9.0	1.9
Actual	66.3	12.6	10.1	9.0	1.8